REDUNDANCY IN THE BIOSYNTHESIS OF TRIACYLGLYCEROL BY *RHODOCOCCUS*

by

Carlos Diaz Salazar Albelda

B.Sc., Pablo de Olavide University, 2010

A THESIS SUBMITTED IN PARTIAL FULFILLMENT OF

THE REQUIREMENTS FOR THE DEGREE OF

MASTER OF SCIENCE

in

THE FACULTY OF GRADUATE AND POSTDOCTORAL STUDIES

(Microbiology and Immunology)

THE UNIVERSITY OF BRITISH COLUMBIA

(Vancouver)

August 2016

ABSTRACT

Many mycolic acid-containing actinobacteria are oleaginous, accumulating high amounts of triacylglycerols (TAGs) under conditions of nutrient stress. These bacteria contain multiple copies of the genes involved in TAG biosynthesis: glycerol-phosphate acyltransferase (GPAT), acylglycerol-phosphate acyltransferase (AGPAT), phosphatidic acid phosphatase (PAP) and diglyceride acyltransferases (WS/DGAT), encoded by *plsB*, *plsC*, *pap*, and *atf*, respectively. Analysis of *Rhodococcus jostii* RHA1's genome revealed that it carries 1 *plsB*, 8 *plsC*, 7 *pap*, and 16 *atf*. Quantitative, time-dependent data of six of these *atf* genes, selected based on previous transcriptomics data, revealed distinct expression patterns under nitrogen-limiting (N^-) and carbon-limiting (C^-) conditions. For example, the levels of *atf10*, *atf3* and *atf8* transcripts dropped ~10-fold upon growth substrate depletion, while the levels of *atf4*, *atf6* and *atf9* transcripts rose. Under N^- conditions, RHA1 cells continued to accumulate TAGs for five days after ammonia depletion, during which time *atf10* and *atf8* transcripts remained abundant. Targeted deletion of any one of *atf3*, *atf4*, *atf6*, *atf9* and *atf10* did not significantly affect TAG accumulation under N^- conditions, consistent with the redundancy of putative acyltransferases in the RHA1 genome. However, deletion of both *atf8* and *atf10* resulted in a 50% decrease in TAG accumulation. Furthermore, the fatty acid profile of the Δ*atf8*Δ*atf10* mutant was significantly perturbed, and was restored by complementation with either *atf8* or *atf10*. RT-qPCR data analysis also revealed that the expression patterns of *plsC* (*RS27555*) and *plsB* were the same as that of *atf9*, consistent with their occurrence in an operon. Unexpectedly, deletion of *plsB* did not affect TAG accumulation, suggesting an alternative pathway for TAG and phospholipids biosynthesis. Finally, I identified three genes encoding HAD-type hydrolases as being putatively involved in TAG biosynthesis, including one that occurs as a fusion with *plsC*. The available data suggest that they act as PAPs. Overall, the results establish that there is a certain degree of functional redundancy in TAG biosynthesis, and that Atf8 and Atf10 play a major role in TAG accumulation. At the same time, the results also highlight important gaps in our knowledge of TAG biosynthesis in mycolic acid-containing oleaginous actinobacteria.

PREFACE

The research presented in this thesis was conducted entirely by Carlos Diaz-Salazar. The research program and experimental design were crafted between Lindsay D. Eltis and Carlos Diaz-Salazar, with additional suggestions from Sawsan Amara. Jie Liu created most of the strains and constructs used in this study. Carlos Diaz-Salazar, Sawsan Amara and Nicolas Seghezzi created the rest of the strains used in this study. Data was analyzed by Carlos Diaz-Salazar and presented following suggestions from Lindsay D. Eltis.

A version of the first half of Chapter 3 (3.1-3.3) has been submitted for publication: Diaz-Salazar C., Roccor R., Amara S., Liu J., and L. D. Eltis. (2016). Breaking down redundancy: the roles of Atf8 and Atf10 in the biosynthesis of triacylglycerols by *Rhodococcus*. Submitted. Diaz-Salazar C. performed the experiments and analyzed the data. Liu J., Diaz-Salazar C., and Amara S. constructed deletion and overexpressing strains. L.D. Eltis and Diaz-Salazar C. wrote the manuscript. L.D. Eltis, Amara S., and Diaz-Salazar C. contributed to the experimental design and discussion.

A version of the second half of Chapter 3 (3.4-3.6) has been published: Amara, S., Seghezzi, N., Otani, H., Diaz-Salazar, C., Liu, J., and Eltis, L. D. (2016). Characterization of key triacylglycerol biosynthesis processes in rhodococci. Scientific Reports **6**: p. 24985. Amara, S., Seghezzi, N., and Diaz-Salazar, C. performed the experiments. Liu J., and Amara S. constructed deletion and overexpressing strains. L.D. Eltis and Amara S. wrote the manuscript. All authors contributed to the experimental design, bioinformatics analysis and discussion. Specifically, Diaz-Salazar, C. performed the RT-qPCR analysis, the bioinformatics analysis of HADs and created Figures 1 and 3 in the manuscript.

TABLE OF CONTENTS

LIST OF TABLES

LIST OF FIGURES

LIST OF ABBREVIATIONS

AGP	Acylglycerol-3-phosphate
AGPAT	Acylglycerol-3-phosphate acyl transferase
C^-	Carbon limited
C/N	Carbon to nitrogen ratio
cDNA	Complementary DNA
CDW	Cellular dry weight
CFU	Colony forming units
DAG	Diacylglycerol
DGAT	Diacylglycerol acyl transferase
DPPA	Dipalmitoyl phosphatidic acid
E. coli	*Escherichia coli*
FA	Fatty acid
FAME	Fatty acid methyl ester
G3P	Glycerol-3-phosphate
GC	Gas chromatography
GPAT	Glycerol-3-phosphate acyl transferase
HAD	Haloacid dehalogenase
IPTG	Isopropyl β-D-1-thiogalactopyranoside
Mtb	*Mycobacterium tuberculosis*
N^-	Nitrogen limited
PA	Phosphatidic acid
PAP	Phosphatidic acid phosphatase
PD630	*Rhodococcus opacus* PD630
RHA1	*Rhodococcus jostii* RHA1
RT-qPCR	Reverse transcription quantitative polymerase chain reaction
TAG	Triacylglycerol
WS	Wax ester synthase
WT	Wild-type

ACKNOWLEDGEMENTS

I would like to express my deepest gratitude to my advisor, Dr. Lindsay D. Eltis, for his continuous supervision and counsel during these two amazing years of scientific studies. I will always be thankful to him for giving me a chance of becoming a member of the Eltis lab in the first place, and providing me with the constant scientific support that has helped me successfully complete this work. I sincerely appreciate the amount of flexibility I had when designing my research aims and all the advice that helped me become a better scientist.

The completion of this could not have been possible without the immense support of the Eltis Lab. I am extremely grateful to James Round and Raphael Roccor for all the fruitful discussions about my project, which have provided me with innumerous ideas for my experiments and have helped me define the future directions of my research. The molecular biology part of my thesis could not have been completed without the expertise of Jie Liu. She has helped me with every technical part of my project during this two years and I cannot be thankful enough for this. All the protein work in this thesis has been completed thanks to the help of Adam Crowe, Kirsten Brown, Eugene Kuatsjah and Dr. Rahul Singh. They taught me the basis about protein purification and characterization and helped me troubleshoot every problem. Finally, I could not have done this work without the support of our lab manager, Jennifer Lian.

I wish to extend my gratitude to the members of my thesis committee, Dr. William W. Mohn and Dr. J. Thomas Beatty. Dr. Mohn and Dr. Beatty have provided me with extremely useful remarks, ideas and new directions for my thesis during these two years. Specially, all the Gas Chromatography work in this thesis has been performed with equipment at the Mohn lab, and I could not have finished it without his support.

I would also like to acknowledge the continuous support of the administrative staff of the Microbiology and Immunology department, in particular of Darlene Birkenhead, which helped me start a successful life in Vancouver, arranged all my transcripts discordances, and made sure everything in my dossier was satisfactory. I am also extremely grateful to all my friends and members of the Department of Microbiology and

Immunology, for providing me with emotional support and extra-academic life that has made my time in Vancouver a sincere blessing.

Last but not least, I wish to acknowledge all the support that I have always received from my family and friends in Spain during these two years of studying abroad. I wish to send a big thank you to my friends that remain in Spain and elsewhere, which have always provided me with a sense of belonging and familiarity whenever I needed it. Finally and most importantly, I could have never made it this far without the help of my parents, grandmother, and aunt, who have made sure I always had everything I needed so I could focus completely on my work and not worry about anything else. Muchas gracias por todo.

1. INTRODUCTION

Mycolic acid-containing bacteria, or mycolata, are a taxon of actinobacteria that include biotechnologically important strains of *Rhodococcus* and *Corynebacterium* as well as the important pathogen, *Mycobacterium tuberculosis* [1, 2]. Many of these bacteria catabolize a remarkably wide range of organic compounds, such as aromatic compounds and steroids [3, 4]. Most mycolata are also oleaginous, accumulating large amounts of triacylglycerols (TAGs) as lipid droplets, a rare example of a bacterial organelle [5-8]. In these bacteria, TAGs have at least two roles: as a structural component of the outer membrane; and to store energy under conditions of stress, such as hypoxia or nitrogen limitation [2, 7, 9, 10]. Under such conditions, TAGs can comprise over 70% of the cellular dry weight (CDW) [10]. In pathogenic mycobacteria, TAG biosynthesis seems to be essential for the pathogenicity and is thus a potential target for novel therapeutics [9, 11, 12]. Non-pathogenic strains have been touted for their ability to transform lignocellulosic biomass to TAGs as a potential source of biodiesel precursors [13-16]. Rhodococcal species such as *Rhodococcus jostii* RHA1 and *Rhodococcus opacus* PD630 (RHA1 and PD630 hereafter) are of particular interest in this respect due to their ability to grow on biomass-derived compounds [3, 17, 18] and have been engineered to degrade a broader range of such compounds [17, 19-22]. In a previous study, RHA1 was shown to accumulate lipids when grown on benzoate, a model lignin depolymerisation compound that is catabolized through the β-ketoadipate pathway to succinate and acetyl-CoA [23, 24].

In mycolata, TAGs are synthesized via the Kennedy Pathway, which comprises four enzymes (**Fig. 1**) [10, 24]. The first two enzymes, a glycerol-3-phosphate *O*-acyltransferase (GPAT), and a 1-acylglycerol-3-phosphate *O*-acyltransferase (AGPAT), encoded by *plsB* and *plsC*, respectively, catalyze the sequential acylation of glycerol 3-phosphate to phosphatidic acid. Phosphatidic acid is dephosphorylated to diacylglycerol (DAG) and finally acylated by a third acyltransferase, a wax ester synthase/DAG *O*-acyltransferase (WS/DGAT), encoded by the *atf* genes. Interestingly, these mycolata often harbor multiple homologs of Kennedy pathway enzymes [15, 24] as reflected in the number of predicted *atf* homologs: *Mycobacterium tuberculosis* (*Mtb*) harbors 15 *atf*

homologs (called *tgs* genes), PD630 contains 17 *atf* homologs, and RHA1 contains 16 *atf* homologs, including three copies of the *atf14* gene [15, 24, 25]. Bacterial WS/DGATs, or Atfs, are not related to their eukaryotic counterparts [26]. The first bacterial DGAT to be described, AtfA from the gram-negative bacterium *Acinetobacter baylyi* ADP1, was characterized by a high promiscuity towards its substrates: the enzyme utilizes a broad range of acyl-CoA donors, as well as both fatty alcohols and diacylglycerols as acceptors [27]. Although Atfs from mycolata share low amino acid sequence identity with AtfA, the putative catalytic motif, HHxxxDG, is conserved [26]. A comprehensive phylogenetic tree of DGATs from different mycolata species can be found in [15].

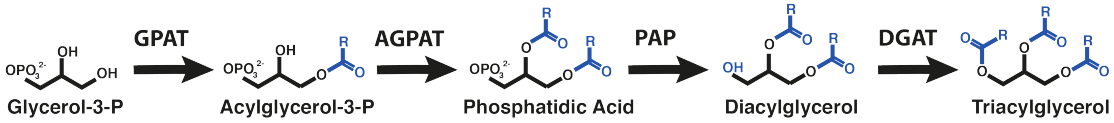

GPATs	PAPs	DGATs	
*plsB (RS27560)**	**Type-2**	*atf1 (RS00140)*	*atf9 (RS27565)*
AGPATs	*RS00400*	*atf2 (RS00145)*	*atf10 (RS30960)*
plsC (RS27555)	*RS15260*	*atf3 (RS00220)*	*atf11 (RS33510)*
plsC2 (RS19670)	*RS24305*	*atf4 (RS00460)*	*atf12 (RS37335)*
RS05380	*RS38180*	*atf5 (RS02840)*	*atf13 (RS38620)*
RS09865	**HAD type**	*atf6 (RS07790)*	*atf14a (RS38695)*
RS10035	*RS19680*	*atf7 (RS14430)*	*atf14b (RS00035)*
RS19675	*RS27555*	*atf8 (RS26160)*	*atf14c (RS35555)*
RS20340	*RS30955*		
RS31620			

Figure 1. The Kennedy pathway of TAG biosynthesis. Top: sequential acylation of glycerol-3-phosphate to form triacylglycerol. **GPAT**, glycerol-3-phosphate acyl transferase; **AGPAT**, acylglycerol-3-phosphate acyl transferase; **PAP**, phosphatidic acid phosphatase; **DGAT**, diacylglycerol acyl transferase. **Bottom:** Homologous genes potentially encoding each enzyme in RHA1.

Several studies have investigated the physiological roles of the various WS/DGATs in rhodococci [15, 18, 28]. However, some of the results are contradictory, and the reasons for the high redundancy of Atf enzymes remain largely unknown. In PD630 cells growing on gluconate under nitrogen-limited conditions, deletion of $atf1_{PD630}$ or $atf2_{PD630}$,

which correspond to *atf3* and *atf6*, respectively, in RHA1, resulted in a 30% to 50% reduction of total fatty acids (FA) compared to the wild-type strain [29, 30]. However, when both genes were deleted together, TAG levels were comparable to those of wild-type PD630, a result that could not be explained by the authors [30]. Clearly, $Atf1_{PD630}$ and $Atf2_{PD630}$ are not equivalent because the former showed significantly higher WS activity than DGAT activity when heterologously produced in *E. coli* [30]. Transcriptomics and proteomics studies in PD630 and RHA1 consistently identify Atf6, Atf8, and Atf10 (RHA1 numbering when no subscripts used) as being highly transcribed and abundant under lipid storage conditions [8, 31, 32]. Moreover, Atf4, Atf6 and Atf8 have been reported to be associated with lipid droplets in PD630 [32]. These results are largely consistent with a recent transcriptomics study showing that *atf8* and *atf10* are highly transcribed under nitrogen-limited (N^-) conditions which promote TAG accumulation, while *atf6*, *atf9*, and *atf4* were the most transcribed *atf* genes under carbon-limited (C^-) conditions [24]. Even though some efforts have been made to characterize the different WS/DGATs, the role of the different homologs in TAG biosynthesis remains poorly understood.

Despite increasing research examining TAG biosynthesis in rhodococci and other mycolata, many aspects of the biosynthetic pathway are still unsolved. TAGs are thought to be synthesized by the Kennedy pathway, which comprises four steps catalyzed by GPAT, AGPAT, PAP2 and WS/DGAT, respectively. The first two enzymes of the Kennedy pathway, GPAT and AGPAT, are encoded by *plsB* and *plsC*, respectively [10]. Most oleaginous mycolata, including RHA1, contain only one copy of *plsB*. In contrast, most of the other TAG biosynthetic enzymes are present in multiple copies. Exceptionally, some *Mycobacterium* species carry a second copy of *plsB* (*Rv1551* in *Mtb*), contiguous to a fatty acid-CoA ligase. Interestingly, the essentiality of *plsB* in mycolata has not been investigated even though most bacteria do not contain a *plsB* homolog in their genomes [33].

The *plsC* gene, encoding the second enzyme of the Kennedy pathway, occurs in 8 copies in the RHA1 genome, two of which are annotated as such (**Fig. 1.1**). Unfortunately, the products of these genes share low sequence identity, which

complicates the study of the physiological relevant AGPAT-encoding genes (data not shown). PAP2, a type 2 phosphatidic acid phosphatase (PAP2), has been proposed to catalyze the dephosphorylation of phosphatidic acid [34]. In support of this, the overproduction of one of the four PAP2 homologs present in RHA1 increased TAG content by 10% of CDW. However, the PAP2's reported activity in *E. coli* membrane extracts was a mere 0.1% of what has been reported for other PAP2s [35]. Moreover, a recent transcriptomics study showed that transcripts of the genes encoding four PAP2 homologs in RHA1 were present at very low abundance under TAG accumulating conditions [24].

In this study, we investigated the contribution of WS/DGATs to TAG accumulation during non-carbon nutritional stress in RHA1. Nutrient utilization, TAG accumulation, fatty acid content and gene expression were monitored in a time-dependent manner. Based on the resulting data, the roles of specific WS/DGATs in TAG biosynthesis were evaluated using mutants deleted in one or more *atf* genes. Furthermore, we performed diverse bioinformatics analyses to examine the genomic arrangement, sequence identity, and domain conservation of GPAT, AGPAT, and potential PAP-encoding genes putatively involved in the Kennedy pathway across representative mycolata species. As part of this, we identified a novel class of PAP-encoding genes and studied their *in vitro* activities. Finally, we investigated the contribution of the contiguous genes *plsC* (*RS27555*) and *plsB* (*RS27560*), as well as the PAP-encoding genes, to TAG accumulation in RHA1. The findings are discussed with respect to the physiology of oleaginous mycolata as well as the implications for biotechnological applications and virulence.

2. MATERIALS AND METHODS

Strains and culture conditions - Strains and plasmids used in this work are listed in Tables 1 and 2, respectively. *E. coli* DH5α was used for DNA propagation. *E. coli* Rosetta™ 2 was used as a host for the overproduction of PapH1 and PapH2. *E. coli* S17.1 was used to conjugate pK18-derived plasmids into RHA1. *E. coli* strains were grown in LB broth at 37 °C, 200 rpm. RHA1 strains were grown at 30 °C in M9 minimal medium containing 20 mM sodium benzoate as sole growth substrate, typically in 250 ml flasks containing 50 ml as previously described [24]. When indicated, benzoate was substituted by glucose (4.2 g/l), sodium gluconate (4.7 g/l) or sodium propionate (2 g/l). Growth media were supplemented with 1 g/l ammonium chloride for nitrogen-excess conditions, and with 0.05 g/l for nitrogen-limitation conditions. Solid growth medium for all strains was LB broth supplemented with Bacto agar (1.5% [w/v]; Difco). Media was further supplemented with 100 μg/ml ampicillin (*E. coli* carrying pTip-derived plasmids), 50 μg/ml kanamycin (*E. coli* carrying pK18-derived plasmids and pET-derived plasmids), 34 μg/ml chloramphenicol (RHA1 carrying pTip-derived plasmids) or 10 μg/ml neomycin (RHA1 carrying pK18-derived plasmids) as appropriate. Expression from the P_{tipA} of pTip-QC2 was induced by adding thiostrepton to a final concentration of 20 μg/ml. Expression from the P_{T7} of pET-41b was induced by adding isopropyl β-D-1-thiogalactopyranoside (IPTG) to a final concentration of 0.5 mM. Bacterial growth in liquid media was routinely measured using optical density at 600 nm. For lipid analysis and RNA extraction, RHA1 cultures were spun down at 3,220 × *g* for 15 min at 4 °C, and pellets were washed with distilled water and stored at -80 °C.

DNA manipulation, plasmid construction, and gene deletions - DNA was isolated, manipulated, and analyzed using standard protocols [36]. Oligonucleotides used in this study are listed in Table S3. RHA1 genes were amplified from genomic DNA using gene-specific primers and GoTaq DNA polymerase (Promega) with standard PCR settings. Amplicons were digested with appropriate restriction enzymes and ligated into pK18*mobsacB* [37] or pTip-QC2 [38] using T4 DNA ligase (Thermo Fisher). DNA was sequenced at Genewiz Inc. pTip-derived plasmids were transformed into RHA1 by electroporation (1.8 kV for 5 ms) using a MicroPulser with GenePulser cuvettes (Bio-

Rad). Genes were deleted in RHA1 using homologous recombination and SacB-based selection as previously described [39]. Briefly, pK18-derived plasmids were electroporated into *E. coli* S17.1 and then conjugated into RHA1. After the second recombination, kanamycin-sensitive/sucrose-resistant colonies were screened and confirmed using PCR.

RNA isolation and RT-qPCR - RHA1 cells were disrupted using a FastPrep-24 bead beater (MP Biomedicals) operated at power 5. Cells were subjected to 6 × 40 s rounds of bead beating with 5 min incubation on ice between rounds, and 20 min incubation at 50 °C after Round 3. Total RNA was extracted using TRIzol® (Invitrogen) reagent and treated with TURBO™ DNase (Invitrogen) to remove genomic DNA. cDNA was synthesized using the SuperScript® VILO cDNA synthesis kit (Thermo Fisher) according to the manufacturer's instructions. RT-qPCR was carried out in duplicate on an ABI stepOnePlus real-time PCR system as previously described using *sigA* (*RHA1_RS33345*) as a reference [24]. Primers and FAM-labelled TaqMan probes (Table 3) were designed using IDT PrimeTime qPCR design tools. Known concentrations of genomic DNA was used to create standard curves for each target gene on each run. Relative cDNA quantity of each target was normalized to that of *sigA* under each condition tested.

Ammonium and benzoate quantification - Spent media from harvested RHA1 cultures were stored at -80 °C and used as appropriate. Ammonium concentrations were determined using an adapted [40] indophenol blue method [24]. To quantify the concentration of benzoate, 100 µl samples were diluted to 500 µl in distilled water and acidified with 20 µl of 3 M HCl. Benzoate was extracted twice by adding 1 ml of ethyl acetate, shaking by hand for 2 min and centrifuging the samples at 2000 × *g* for 5 min. The organic phase was recovered, dried under N_2 stream, resuspended in 100 µl pyridine, and derivatized with 100 µl BSTFA-1%TMCS (Supelco) for 20 min at 60 °C. Samples were analyzed using an Agilent 6890 series gas chromatograph (GC) equipped with an HP-5 MS 30 m × 0.25 mm capillary column (Hewlett-Packard) and an HP 5973 mass-selective detector. Helium was used as the carrier gas with a flow rate of 1 ml/min. The

GC was operated on split-less mode with an injector temperature of 280 °C. The temperature program of the oven was 80 °C for 3 min, increased to 290 °C at a rate of 15 °C per min, and then held at 290 °C for 10 min. The mass spectrometer was operated in electron emission scanning mode at 40 to 800 *m*/*z* and 1.96 scans per second. For quantitative analysis, tridecanoic acid was used as internal standard.

Phosphatidic acid phosphatase activity assay – Phosphatidic acid phosphatase activity of purified PapH1 was measured using the malachite green assay [41]. Briefly, the dephosphorilation of 200 μM of dipalmitoyl phosphatidic acid (Sigma) in reaction buffer (25mM Tris-HCl, 50mM KCl, 20mM $MgCl_2$, pH 7,4) was started with the addition of 50 μl of purified PapH1. After 30 min of incubation at 30 °C, malachite green reagent was added (1 mM Malachite green, 8.5 mM Ammonium Molybdate, 0.1% Triton-X100 in 1M HCl). Colour was quenched by adding 34% citric acid solution 1 minute after, and absorbance was read at 640 nm. A standard courve was prepared with 0-500 μM inorganic phosphate.

Lipid analysis, FA profiling, and statistical analysis - Total fatty acids were quantified in freeze-dried whole cells as described previously [42] and was used as a proxy for TAGs [30]. Briefly, 4 mg of lyophilized cells were resuspended in 1 ml toluene and subjected to methanolysis with 2 ml acidic methanol (15% v/v sulfuric acid) for 2 h at 100 °C. The mixture was brought to room temperature, neutralized by adding 2 ml of saturated sodium bicarbonate aqueous solution, and phases were allowed to separate overnight. Fatty acid methyl esters (FAMEs) were recovered in the organic phase, dried under a N_2 stream and suspended in 1 ml hexane. Samples were diluted 1:10 to 1:100 and analyzed on GCMS. The temperature program of the oven was 90 °C for 2 min, increased to 150 °C at a rate of 15 °C per min, then increased to 250 °C at a rate of 5 °C per min, the held at 250 °C for 3 min. The mass spectrometer was operated in electron emission scanning mode at 40 to 800 *m*/*z* and 1.96 scans per second. Tridecanoic acid was used as internal standard. Identification and quantification of the peaks was performed using software packages including GCsolution Analysis v.2.32, GCMS Solutions v.2.53 (Shimadzu Scientific Instruments, Columbia, MD), and the NIST08 Library.

Only FA species that comprised more than 2% of total FAs present in the wild-type strain were reported and considered for statistical analysis. For each species studied, the variance in the replicates of each strain was summed and divided by the number of different strains used in the analysis. This pooled variance was termed α. The variance in the means of the replicates for each strain was defined as β. Finally, the average of these means, γ, was used to determine the relative abundance of each FA species among all FAs species analyzed. FA species datasets where $\alpha*\beta/\gamma$ was greater than 0.5 were further analyzed using a significance level of 0.05.

Table 1. Bacterial strains used in this work

Strain	Description	Reference or source
E. coli		
DH5α	*E. coli* K-12 ϕ80d*lacZ*ΔM15 (*F-lac*U169) *recA*1 *endA*1 *hsdR*17 (r_k^- m_k^+) *deoR supE*44 *thi*-1 *gyrA96 relA*1	[43]
S17.1	*E. coli* K-12 *pro*, *hsdR*17 (r_k^- m_k^+), *res*$^-$, *RP4-2-Tc::Mu-Km::Tn7, Tp*^{r}, *Sm*^{r}	[44]
Rosetta™ 2	*F*$^-$ *ompT hsdS*$_B$*(r*$_B^-$ *m*$_B^-$*) gal dcm pRARE2 (Cam*^{R}*)*	Millipore
RHA1		
RHA1	Wild type/ Parental strain[a].	[45]
Δ*atf3*[b]	*atf*3 deletion mutant of RHA1	This study
Δ*atf6*	*atf*6 deletion mutant of RHA1	This study
Δ*atf8*	*atf*8 deletion mutant of RHA1	[24]
Δ*atf9*	*atf*9 deletion mutant of RHA1	This study
Δ*atf10*	*atf*10 deletion mutant of RHA1	This study
Δ*atf6*Δ*atf9*	RHA1_Δ*atf6* derivate with *atf9* gene deletion.	This study
Δ*atf8*Δ*atf10*	RHA1_Δ*atf8* derivate with *atf10* gene deletion.	This study
Δ*atf6*Δ*atf8* Δ*atf9*	RHA1_Δ*atf6*Δ*atf9* derivate with *atf8* gene deletion.	This study
Δ*atf8*Δ*atf9* Δ*atf10*	RHA1_Δ*atf8*Δ*atf10* derivate with *atf9* gene deletion.	This study
RHA1_Δ*plsB*	*plsB* deletion mutant of RHA1	This study
RHA1_Δ*plsC*	*plsC* deletion mutant of RHA1	This study
RHA1_Δ*papH1*	*papH1* deletion mutant of RHA1	This study

[a] All RHA1 strains are naturally resistant to nalidixic acid.

Table 2. Plasmids used in this study

Plasmid	Description	Reference or source
pK18*mobSacB*	Conjugative suicide vector for gene mutagenesis in Rhodococcus; *Km*^{r} *aphII sacB* oriT (RP4) *lacZ*	[37]
pTip-QC1	Expression vector for *Rhodococcus* with P*tipA* promoter, *repAB* (pRE2895); *Cm*^{r}, *Km*^{r}	[38]
pTip-QC2	Expression vector for *Rhodococcus* with P*tipA* promoter, *repAB* (pRE2895); *Cm*^{r}, *Km*^{r}	[38]
pET-41b	Expression vector for *E. coli* with P_{T7} promoter, GST-Tag, His-Tag; *Neo*^{r}, *Km*^{r}	[46]
pTip_His-*plsC*	pTip-QC1 bearing the *plsC* gene with a N-terminal HisTag under the P*tipA* promoter	This study
pTip_*atf3*	pTip-QC2 bearing the *atf3* gene under the P*tipA* promoter	This study
pTip_*atf6*	pTip-QC2 bearing the *atf6* gene under the P*tipA* promoter	This study
pTip_*atf8*	pTip-QC2 bearing the *atf8* gene under the P*tipA* promoter	[24]
pTip_*atf10*	pTip-QC2 bearing the *atf10* gene under the P*tipA* promoter	This study
pTip_*plsC*	pTip-QC2 bearing the *plsC* gene under the P*tipA* promoter	This study
pTip_*papH1*	pTip-QC2 bearing the *papH1* gene under the P*tipA* promoter	This study
pTip_*papH2*	pTip-QC2 bearing the *papH2* gene under the P*tipA* promoter	This study
pK18_*atf3*KO	pK18*mobSacB* plasmid carrying *atf3* flanking regions cloned into MCS with *Xba*I-*Eco*RI-*Hind*III	This study
pK18_*atf6*KO	pK18*mobSacB* plasmid carrying *atf6* flanking regions cloned into MCS with *Xba*I-*Nde*I-*Hind*III	This study
pK18_*atf8*KO	pK18*mobSacB* plasmid carrying *atf8* flanking regions cloned into MCS with *Xba*I-*Bam*HI-*Hind*III	[24]
pK18_*atf9*KO	pK18*mobSacB* plasmid carrying *atf9* flanking regions cloned into MCS with *Eco*RI-*Nde*I-*Bam*HI	This study

Plasmid	Description	Reference or source
pK18_*atf10*KO	pK18*mobSacB* plasmid carrying *atf10* flanking regions cloned into MCS with *Eco*RI-*Hind*III-*Xba*I	This study
pK18_*plsB*KO	pK18*mobSacB* plasmid carrying *plsB* flanking regions cloned into MCS with *Eco*RI-*Nde*I-*Xba*I	This study
pK18_*plsC*KO	pK18*mobSacB* plasmid carrying *plsC* flanking regions cloned into MCS with *Bam*HI-*Xba*I-*Hind*III	This study
pK18_*papH1*KO	pK18*mobSacB* plasmid carrying *papH1* flanking regions cloned into MCS with *Eco*RI-*Hind*III (Gibson's assembly)	This study
pET_*papH1*	pET-41b bearing the *papH1* gene with a N-terminal HisTag under the P_{T7} promoter	This study
pET_*papH2*	pET-41b bearing the *papH2* gene with a N-terminal HisTag under the P_{T7} promoter	This study

Table 3. Oligonucleotides used in this study

Oligo name	Nucleotide sequence[a]
Construction of gene deletion mutants	
***atf3*-up-F**	GCTCTAGAGCACGGTTGGACACTGGTAGCACG
***atf3*-up-R**	CGGAATTCCCACGACATGAAGTCCGTCTGGG
***atf3*-dn-F**	TTGAATTCGAGTCTCTCGCCGACGGGTTTCG
***atf3*-dn-R**	TTTAAGCTTGAGCGCCTCGATCAGTTGGTCG
***atf6*-up-F**	GACCATTTCTAGACGTAGACCATTTCCTGCGAG
***atf6*-up-R**	CGATAGACATATGGAACAATTCGAGCGATCCCAC
***atf6*-dn-F**	CTGAATCCATATGCAGCGCATCCTCTTCTATCTC
***atf6*-dn-R**	CGAAAGCTTGGTGAGTTCGTGTCGGTGATC
***atf8*-up-F**	GCTCTAGACGGCAGTTCGGACGCTCGGTAC
***atf8*-up-R**	TTGGATCCGGACTCGCCGAGAAGGAACATCG
***atf8*-dn-F**	TTGGATCCGTGCCCGACCTGAAGTCGATCC
***atf8*-dn-R**	TTTAAGCTTGACGGCCTGGATCTTCTCGTTGG
***atf9*-up-F**	GCTATGAATTCGCTCGACCTTCAGTTCACC
***atf9*-up-R**	GGTCATATGTATCAGAGGTTCGCCGTC
***atf9*-dn-F**	GAGCATATGGAGATCGTCGAACTGGGC
***atf9*-dn-R**	CTAGGATCCGGTTGAGCGGAAGATCGTTC
***atf10*-up-F**	CGGAATTCCGTCGCGACACCGAGTCGCCG
***atf10*-up-R**	CCCAAGCTTGAAGATCGCGAGCGATCCCAC
***atf10*-dn-F**	CCCAAGCTTAATGCAGACCGTGATGCCATG
***atf10*-dn-R**	GCTCTAGAAGACCGATGCCGATGTACTGG
***plsB*-up-F**	GCTATGAATTCCAGGCACTCGACAACGTG
***plsB*-up-R**	GGTCATATGCTCGATGAGGTAGACCCG
***plsB*-dn-F**	GAGCATATGGAGAATCTCGACCAGATGGGT
***plsB*-dn-R**	GACTTGTCTAGAGGTTCTGGGTGAGCAGTC
***plsC*-up-F**	TCTGGATCCGCGATGTGGACCTGACCGATCC
***plsC*-up-R**	GTCTCTAGAGTCCAGATCGAACGCGGCGAG
***plsC*-dn-F**	TTCTCTAGATGGAACCTCGCGGATCTCGACC
***plsC*-dn-R**	TGTAAGCTTCCAGGTATTCGACCACCATCCGC
***papH1*-up-F**	GCTATGACATGATTACGAATTCAGGACGGCAACGCCC AGCTC
***papH1*-up-R**	ATCTCGTCCGACAGGCCGTCCATGTCCG
***papH1*-dn-F**	GCCTGTCGGACGAGATAGCGATACTTCTCGAGG
***papH1*-dn-R**	CGACGGCCAGTGCCAAGCTTCGCGTTCAGCGGACTCG

Oligo name	Nucleotide sequence[a]
Overexpression of genes in RHA1	
***atf3*-ex-F**	ACGAGCCATATGACCGACGTGATCACCAC
***atf3*-ex-R**	ACGAGCGAATTCTCATGAGGCCACGACCACCC
***atf6*-ex-F**	ACGAGCCATATGCCGGTTACCGATTCGAT
***atf6*-ex-R**	ACGAGCGAATTCTCAGAGCAATGCCGCCTCGA
***atf8*-ex-F**	ACGAGCCATATGCCGCTCCCCATGTCCCC
***atf8*-ex-R**	ACGAGCGAATTCTCAGATTCCGACCGCGCGCT
***atf10*-ex-F**	ACGAGCCATATGGTGACGAGACTGACTAC
***atf10*-ex-R**	ACGAGCGAATTCTCACCGGCTGGCATCCAACA
***plsC*-ex-F**	GAACCACATATGATGAGCGATCTCCGCAGTCT
***plsC*-ex-R**	GAACAGGAATTCGAGATCTTTCAGCGATGCCC
***papH1*-ex-F**	GACTCGCATATGGTGCGGGGATTGATATTGG
***papH1*-ex-R**	GAATAGGAATTCTCACCATGTCGGCGCCT
***papH2*-ex-F**	GAATAACATATGGTGAGCCCAGACCGACCGA
***papH2*-ex-R**	GAACAGGAATTCTCTCAGGACCACCAGCG
confirmation of the *atf9-plsB-plsC* operon	
Pair1-F	CAGGACAGTCTCGACGAGATC
Pair1-R	CTTTGACACCTTGTACTGCGTG
Pair2-F	GGGAAGCGAATCTGGGTGA
Pair2-R	CGATGTCGTCGTGGAGACT
Pair3-F	CTGTTCGAGGACTGCCTGCA
Pair3-R	GGTTCCGTCGAAATGGTCGAAGG
Pair4-F	CATGACCATGATCGCCGAAGTCC
Pair4-R	CCTGCTGTGTCGATGAGGAACC
Overexpression of ht-PlsC in RHA1	
***ht-plsC*-ex-F**	GAACCACATATGATGAGCGATCTCCGCAGTCT
***ht-plsC*-ex-R**	GAACAGGAATTCGAGATCTTTCAGCGATGCCC
Overexpression of ht-PapH1 and ht-PapH2 in *E. coli*	
***ht-papH1*-ex-F**	GAACCATATGGCTACTAGTCATCACCATCACCATCACGG CAGCTCTGAGAACCTGTACTTCCAGTCGCGGGGATTGAT ATTGGACTTCGG
***ht-papH1*-ex-R**	CCCAAGCTTTCACCATGTCGGCGCCTGTCC
***ht-papH2*-ex-F**	GAACCATATGGCTACTAGTCATCACCATCACCATCACGG CAGCTCTGAGAACCTGTACTTCCAGTCGAGCCCAGACCG ACCGAGCCTTG
***ht-papH2*-ex-R**	CCCAAGCTTTCAGGACCACCAGCGCTCGAGC

Oligo name	Nucleotide sequence[a]
RT-qPCR	
***atf3*-F**	GATTCCGTTTTCCCCGATGA
***atf3*-R**	GTGTTTGAGCATGTTTCCGAG
***atf3*-probe**	CCTGCTTCCCGCCTCGACA
***atf4*-F**	TGATGATCTCGTACATGCCG
***atf4*-R**	GTGAGGGTGATGCTGAGTG
***atf4*-probe**	AGGCCGCGATACTGGAATGGG
***atf6*-F**	GAAGACCATGTACTGGAACGG
***atf6*-R**	TGGTGAGCGTGATGTTGAG
***atf6*-probe**	CGGCTGGACGGCATCTACCC
***atf8*-F**	GGAGCTGATGGCACTCTG
***atf8*-R**	GTGGATCTTGGTGTAGACGG
***atf8*-probe**	CTGATCGAGGGACTGGGCGAC
***atf9*-F**	ACATGGTGCCGCGTATC
***atf9*-R**	GACAAGTGATAGTCGAGGTCG
***atf9*-probe**	CCACATCGGATTGCCCAGCC
***atf10*-F**	AGCGGATGTTCAACCTGATG
***atf10*-R**	ACCGATGCTCAAAGTCTGG
***atf10*-probe**	AGCGCGGATGCTCGAGATGT
***sigA*-F**	CTGATCCAGGAAGGCAACC
***sigA*-R**	AGAACTTGTAGCCCTTGGTG
***sigA*-probe**	CGAACTTCTCGACGGCACGGAT

[a] enzyme restriction sites are shown underlined

3. RESULTS

1. Integrated analysis of TAG accumulation dynamics in RHA1

To better understand the relationship between nutrient consumption, lipid production and the expression of TAG biosynthetic genes in oleaginous mycolata, we monitored these parameters in a time-dependent manner in RHA1. We based these experiments on our transcriptomics studies in which we used 20 mM benzoate to model lignin depolymerisation products and either 0.05 or 1 g/l (0.93 and 18.7 mM) ammonium chloride [24], representing N^- and C^- conditions, respectively. Under C^- conditions, RHA1 grew exponentially until benzoate was depleted, at which point the cells entered stationary phase and ammonium ceased to be consumed (**Fig. 2**). The growth yield (CDW) was 0.76 ± 0.06 mg/ml and the TAG content was maximal (15% CDW) at early stationary phase. This decreased to 4% CDW 125 h after the benzoate was consumed. Under N^- conditions, TAGs, as measured by total FAs, began accumulating when ammonium levels dropped below 0.15 mM, reaching a maximum of 50% CDW at 160 h, approximately 120 h after the ammonium was depleted from the culture medium. Benzoate consumption continued during this time, with the growth yield increasing from 0.05 ± 0.01 mg/ml at 30 h to 0.37 ± 0.02 mg/ml at 160 h. Over this same time, cell numbers increased from 1×10^7 to 1×10^8 CFU, plateauing after 100 h. Over 8% of the consumed benzoate was finally converted to TAGs. Under both C^- and N^- conditions, the cultures were initially at pH 7.0, and remained at this value throughout growth.

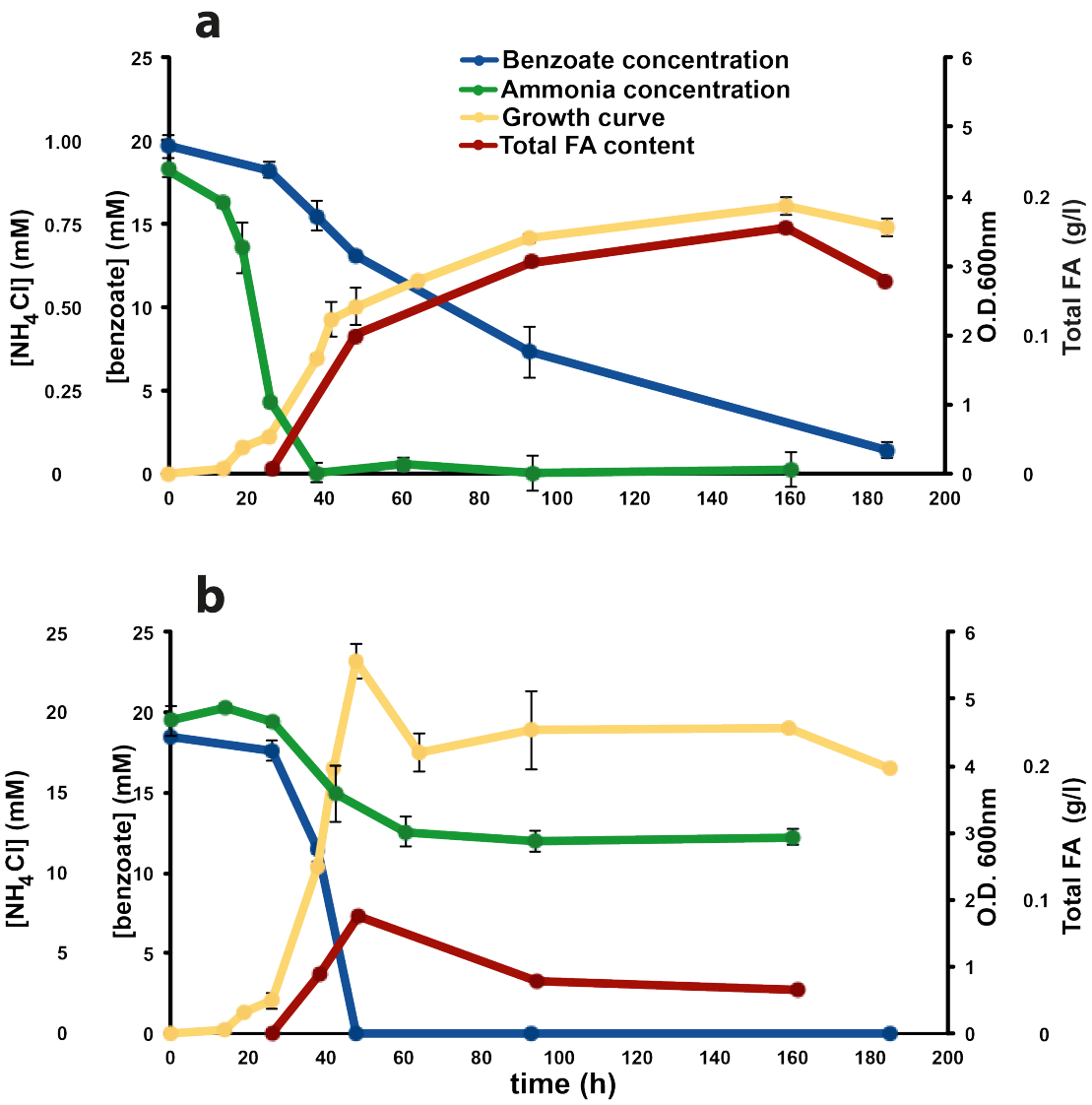

Figure 2. TAG accumulation dynamics. Time dependent evolution of optical density (yellow), ammonia (green) and benzoate (blue) concentration in spent media, and total FAs (red) in a culture of RHA1 grown under Nitrogen limiting (a) or excess (b) conditions.

Concurrently, we used RT-qPCR to establish the time-dependent expression profiles of *atf* genes previously reported to be implicated in TAG biosynthesis in rhodococci [8, 24, 29-32]: *atf3*, *atf4*, *atf6*, *atf8*, *atf9*, and *atf10* (**Fig. 3**). Under C^- conditions, the expression pattern of these genes changed upon benzoate depletion: the *atf4*, *atf6*, and *atf9* transcripts increased 7- to 29-fold in abundance, while those of *atf3*, *atf8*, and *atf10* decreased 4- to 13-fold. Among those that increased, the *atf6* transcripts decreased ~5-

fold as stationary phase progressed while the *atf9* transcripts continued to increase in abundance. Under N^- conditions, only the *atf8* and *atf10* transcripts were highly abundant initially, and these levels dropped ~2-fold in the 40 h following ammonium depletion. None of the other *atf* genes appeared to be significantly transcribed, although the levels of *atf4* transcripts increased slightly as TAGs accumulated. Overall, the relative expression levels of each *atf* gene were largely consistent with our previous transcriptomic studies [24]. Nevertheless, the RT-qPCR data establish that *atf10* transcripts were the most abundant under all conditions. That is, the values in the different Figure 3 panels may be compared with each other because all transcript levels were normalized to *sigA* transcripts. More specifically, the high abundance of *atf10* and *atf8* transcripts during TAG accumulation (*i.e.*, after ammonium depletion) combined with their relatively low abundance during TAG depletion (*i.e.*, after benzoate depletion) suggest that Atf8 and Atf10 play a significant role in synthesizing TAG for storage.

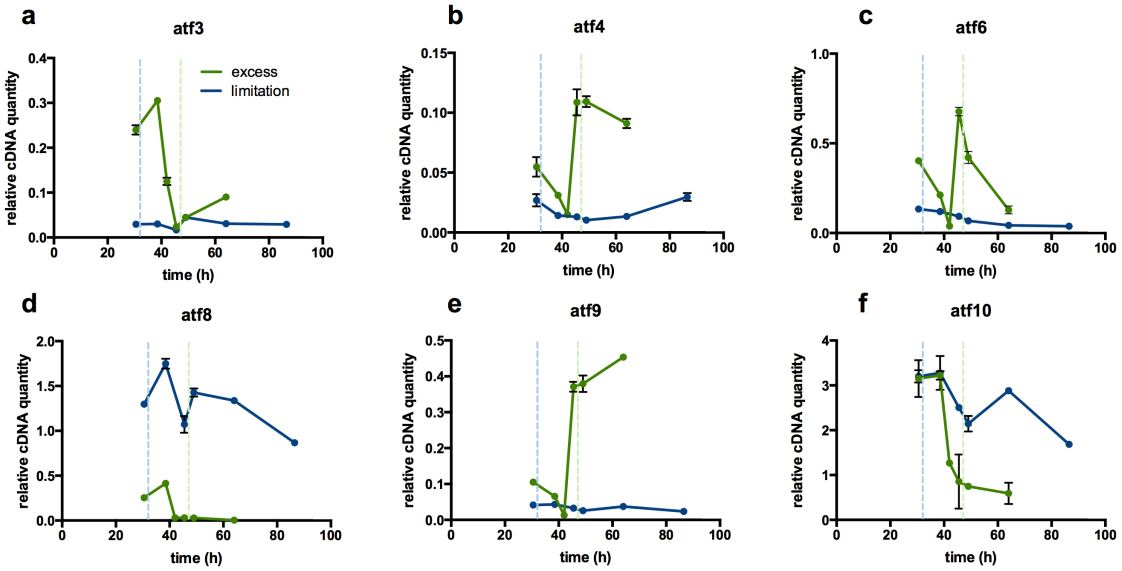

Figure 3. RT-qPCR analysis of *atf* transcripts. RHA1 cells were grown on 20 mM benzoate as sole growth substrate under either nitrogen-limited (blue) or carbon-limited (green) conditions. Dashed lines denote the point at which ammonia (light blue) or benzoate (light green) were depleted, respectively. Relative cDNA quantity indicates the level of each transcript standardized to the level of *sigA* transcript under each condition.

To determine whether the observed gene expression profiles were growth substrate-dependent, we measured transcript levels in cells growing on different carbon sources as they entered stationary phase (**Fig. 4**). More specifically, RHA1 was grown under N^- and C^- conditions on each of glucose and gluconate using carbon loads corresponding to 20 mM benzoate as well as on propionate at lower concentrations to avoid toxicity. Overall, the levels of *atf* transcripts were independent of the carbon source. Similarly, the TAG content of RHA1 cells grown on these carbon sources was comparable to the TAG content of cells grown on benzoate (~50% CDW in N^- and ~13% CDW in C^- conditions), although growth on gluconate promoted slightly higher accumulation of TAGs (~60% CDW in N^- conditions).

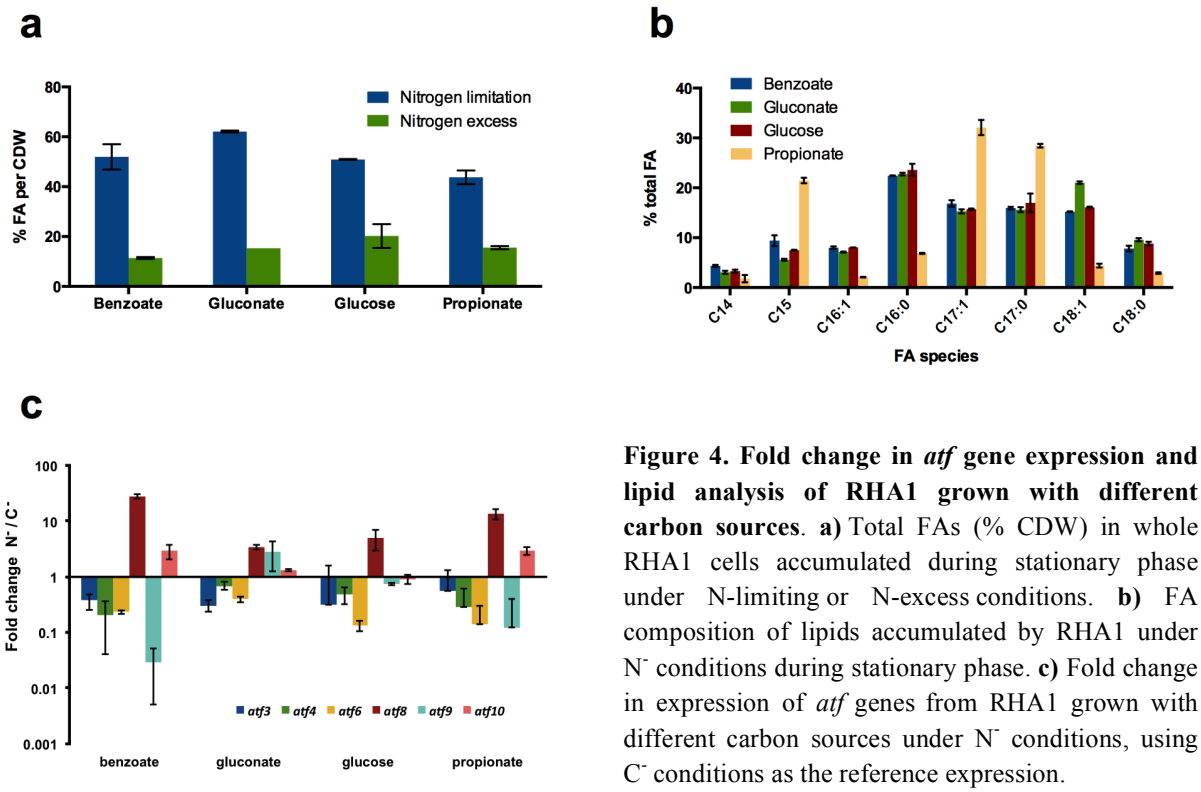

Figure 4. Fold change in *atf* gene expression and lipid analysis of RHA1 grown with different carbon sources. **a)** Total FAs (% CDW) in whole RHA1 cells accumulated during stationary phase under N-limiting or N-excess conditions. **b)** FA composition of lipids accumulated by RHA1 under N^- conditions during stationary phase. **c)** Fold change in expression of *atf* genes from RHA1 grown with different carbon sources under N^- conditions, using C^- conditions as the reference expression.

2. A redundant system for TAG biosynthesis in RHA1: role of *atf8* and *atf10*

The time-dependent expression profiles led us to hypothesize that Atf8 and Atf10 are the main WS/DGATs contributing to TAG storage. To gain more insight into the role of *atf* genes in TAG accumulation, we ectopically overexpressed them in wild-type RHA1 using a titratable promoter and investigated their influence under N^- conditions. Consistent with our previous report [24], overexpression of *atf8* increased TAG content by 10% (**Fig. 5**). By contrast, overexpression of other *atf* genes either negatively impacted TAG accumulation (*atf3* and *atf10*) or had no observable effect (*atf6*).

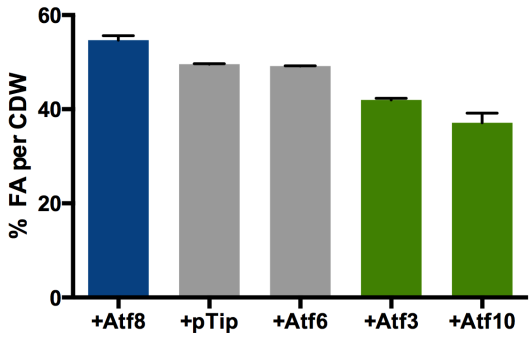

Figure 5. Percentage of FA per CDW of wild-type RHA1 overproducing Atf enzymes. Cells were cultured under nitrogen-limited conditions and harvested 50h after ammonia was depleted. Blue indicates strains that accumulate higher amounts of TAGs. Green indicates strains accumulating fewer TAGs.

To further investigate the physiological relevance of *atf* genes, we used homologous recombination to construct deletion mutants of *atf* genes that were highly abundant under either N^- or C^- conditions (**Fig. 3**). Comparison of their TAG accumulation phenotype 60 h after ammonia was depleted, as measured by total FA content, revealed that deletion of any single gene did not significantly affect TAG accumulation under N^- conditions (**Fig. 6**). This finding is consistent with the high redundancy of putative WS/DGATs encoded by the RHA1 genome. Interestingly, deletion of either *atf8* or *atf10* resulted in lower TAG accumulation under C^- conditions at stationary phase. By contrast, deletion of either *atf3*, *atf6*, or *atf9* had no effect on TAG accumulation under C^- conditions. Finally, the single gene deletion mutants grew with the same kinetics as WT RHA1 (data not shown).

We hypothesized that the lack of an observable phenotype on TAG accumulation (*i.e.*, under N^- conditions) in single deletion mutants was due to the functional redundancy of *atf* genes in RHA1. To test for such redundancy, we constructed two double deletion mutants: Δ*atf8*Δ*atf10* and Δ*atf6*Δ*atf9*. The former represent the most abundant *atf* transcripts during N^- TAG accumulation while the latter represent the two transcripts that increased most in abundance upon benzoate depletion (**Fig. 3**).

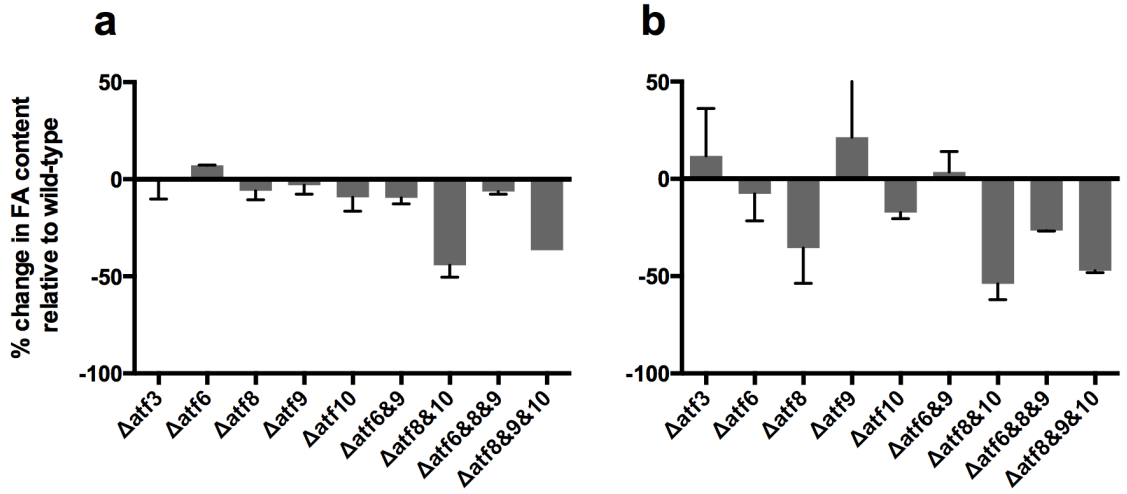

Figure 6. Total FA accumulation in *atf* gene deletion mutants. RHA1 strains were grown on 20 mM benzoate as sole growth substrate under either nitrogen-limited (N^-) or carbon-limited conditions (C^-). Cells were harvested at 60h after ammonia was depleted for N^- cultures, and 30h after benzoate was exhausted for C^- cultures. **a)** FA content of single, double and triple *atf* mutants under N^- conditions. **b)** FA content of the same *atf* mutants under C^- conditions. FA content of each strain was standardized to that of the wild-type strain under the same culture conditions.

Deletion of *atf8* and *atf10* resulted in a ~50% decrease in TAG content compared to wild-type RHA1 under both the N^- and C^- conditions sampled above (**Fig. 6**). This result indicates that Atf10 and Atf8 play at least partially redundant roles in TAG accumulation. By contrast, the Δ*atf6*Δ*atf9* double mutant did not have any defect in TAG accumulation under either condition tested (**Fig. 6**). Finally, deletion of *atf9* in the Δ*atf8*Δ*atf10* background did not change the phenotype of the Δ*atf8*Δ*atf10* mutant. In addition, deletion of *atf8* in the Δ*atf6*Δ*atf9* background yielded the Δ*atf8*Δ*atf9*Δ*atf10* mutant, which had a similar phenotype as the Δ*atf8* single mutant (**Fig. 6**). Overall, the data indicate that *atf8* and *atf10* play somewhat redundant roles in TAG accumulation in RHA1, but that neither *atf6* nor *atf9* are essential for TAG accumulation under any of the conditions tested.

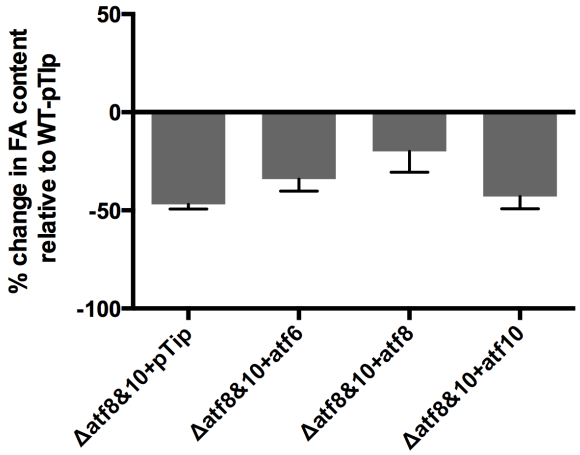

Figure 7. FA content of the Δ*atf8&10* strain complemented with different Atf enzymes. Strains were grown under N^- conditions and harvested 50 h after ammonia depletion. FA content was standardized against the WT strain harboring an empty pTipQC2 expression plasmid.

To additionally test the role of *atf8* and *atf10* in TAG accumulation, we complemented the Δ*atf8*Δ*atf10* double mutant with either *atf8*, *atf10*, or *atf6*, using the same strategy as described above. A pTip plasmid expressing Atf8 restored TAG content in the double mutant to levels comparable with wild-type RHA1 bearing an empty vector (**Fig. 7**). By contrast, complementation with *atf6* or *atf10* failed to rescue the TAG-deficient phenotype of the Δ*atf8*Δ*atf10* mutant.

3. Perturbation of FA composition of TAGs in RHA1

In RHA1 under N^- conditions, odd-numbered FAs ($C_{15:0}$, $C_{17:0}$ and $C_{17:1}$) comprised ~40% of total FAs in cell grown on benzoate, glucose or gluconate (**Fig. 4**). When RHA1 was grown on propionate, the percentage of odd-numbered FAs increased to ~75% of total FAs, presumably because propionyl-CoA is a precursor for the biosynthesis of odd-number FAs (**Fig. 4**) [47]. Overexpression of Atf8 in RHA1 increased the percentage of odd-numbered FAs ($C_{15:0}$ and $C_{17:0}$) while decreasing the percentage of $C_{18:1}$ FA (**Fig. 8**). No other Atf enzyme that was tested perturbed the FA profile of RHA1 when overproduced. Moreover, all of the single *atf* deletion mutants had normal FA profiles, consistent with the high redundancy of putative DGATs in RHA1. By contrast, the Δ*atf8*Δ*atf10* double mutant had a FA profile that was perturbed in a manner opposite to that of the *atf8* overexpressing strain: decreased $C_{15:0}$ and $C_{17:0}$ content and an increased $C_{18:1}$ content (**Fig. 8**). Consistent with the TAG accumulation phenotype, the Δ*atf8*Δ*atf9*Δ*atf10* triple mutant had the same FA profile as the Δ*atf8*Δ*atf10* double

mutant. Furthermore, the Δ*atf6*Δ*atf9* double mutant and the Δ*atf6*Δ*atf8*Δ*atf9* triple mutant had normal FA profiles. Finally, complementation of the Δ*atf8*Δ*atf10* double mutant with *atf10* restored the FA profile to that of wild-type RHA1 (**Fig. 8**), while complementation with *atf6* led to a partial recovery. Interestingly, complementation with *atf8* yielded an FA profile similar to that of the Atf8-overexpressing wild-type strain.

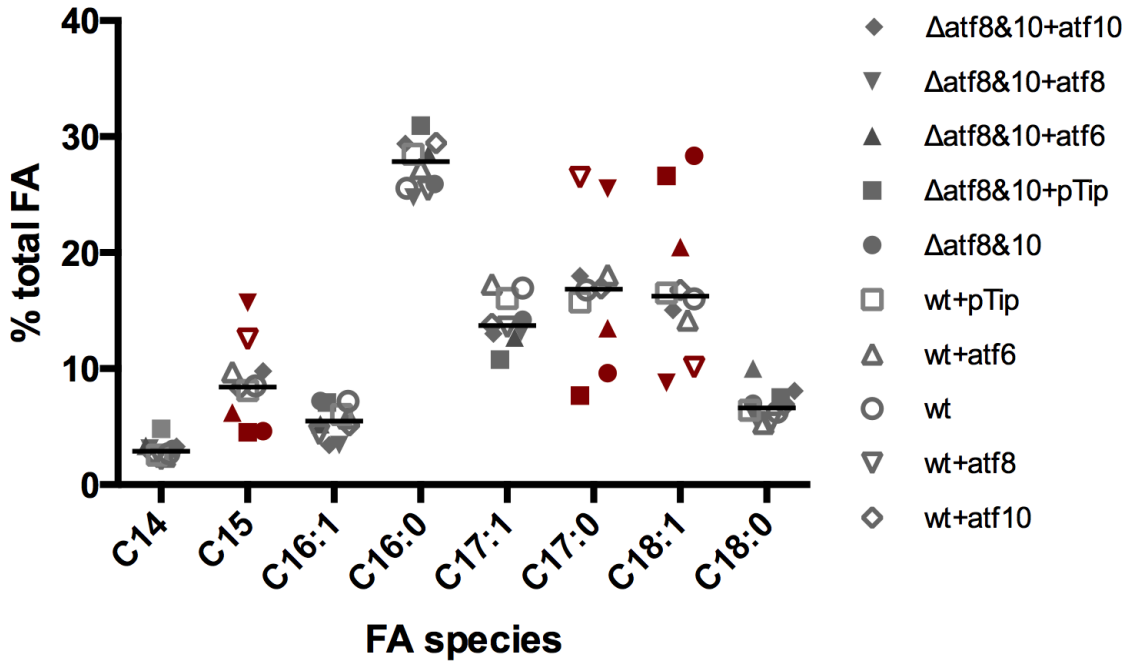

Figure 8. FA profiles of wild type RHA1 and mutants involving *atf8* and *atf10*. Wild-type and mutant strains were complemented with *atf* genes using pTipQC2 and induced with thiostrepton. Cells were grown with benzoate as sole carbon source under conditions of nitrogen limitation. Significant data points ($p<0.05$) are coloured red.

4. Bioinformatic analysis of genes putatively involved in the Kennedy pathway

RT-qPCR data analysis of TAG-related genes revealed that the time-dependent expression profile of *plsC* (*RS27555*) and *atf9* was remarkably similar, thus suggesting a common transcription mechanism (**Fig. 3**). Indeed, *atf9* and *plsC* were shown to be clustered in the same genomic region as *plsB* and a lipid transporter protein, *ltp1* [48]. Using gene specific primer pairs aligning at the juncture between each gene, and complementary DNA (synthesized from single stranded RNA from RHA1), we confirmed via PCR that *atf9* (*RS2765*), *plsB* (*RS2760*), and *plsC* (*RS2755*) were co-transcribed, suggesting that they were arranged in an operon (**Fig. 9**). However, *ltp1* was not co-transcribed with the former genes, suggesting that it does not belong to the same operon. The identification of this operon is noteworthy since most TAG-related genes are not clustered together. Moreover, analysis of representative mycolata genomes indicated that this operon appears to be conserved in genera such as *Rhodococcus, Gordonia, Mycobacterium,* and *Nocardia*, which have been shown to accumulate TAGs under conditions of nutritional stress [7, 47, 49, 50].

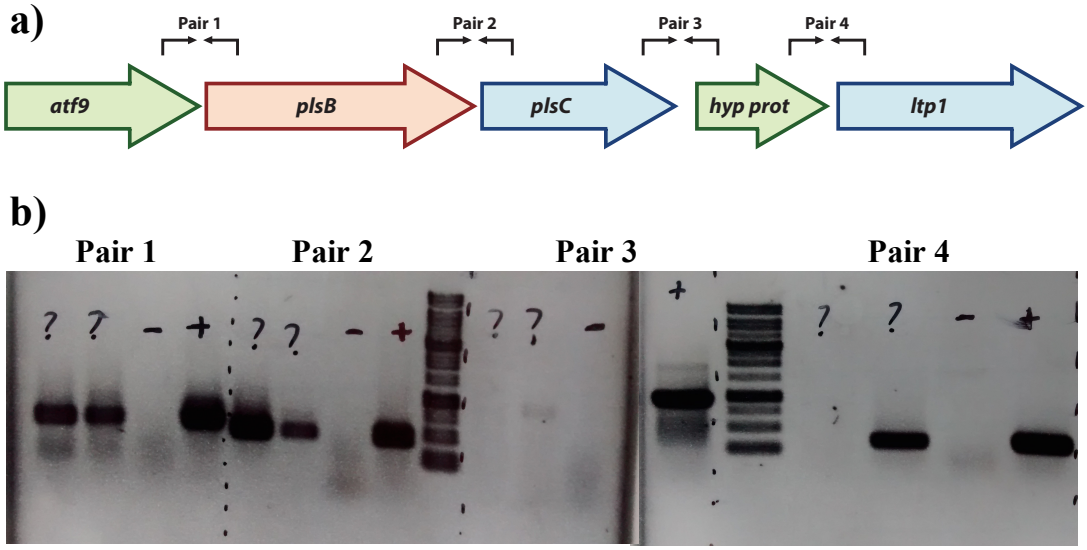

Figure 9. Strategy followed to confirm the operonic conformation of the *plsC* genomic region. **a)** Design of primer pairs (black arrows) to align at the juncture between each gene (thick coloured arrows). Neither genes nor primers are drawn to scale. **b)** Agarose gel image of the PCR of each primer pair using the following templates: "?", RHA1 cDNA template (two replicates). "-", RHA1 RNA template (negative control), "+" RHA1 genomic DNA template (positive control).

The *atf9-plsB-plsC* operon encodes three of the four enzymes of the Kennedy pathway, including the only predicted GPAT encoded by the RHA1 genome. Inspection of the protein encoded by *plsC* revealed that it comprises two domains: an AGPAT domain and a domain belonging to the haloacid dehalogenase superfamily (HAD) (**Fig 10**). Despite their name, several studies have reported HAD-type hydrolases as phosphatases [51, 52]. The possibility that the HAD domain from *plsC* acts as a phosphatidic acid phosphatase would mean than a single, conserved operon encodes all the enzymes required for TAG biosynthesis. Analysis of the genomic context of other TAG-related genes revealed that two other genes encoding predicted HAD hydrolases occur in putative operons with genes from the Kennedy pathway: *RS16980* with *plsC2* (*RS16970*) and *RS30955* with *atf10* (*RS30960*). The protein products of *RS30955* and *RS16980* were called PapH1 and PapH2, respectively, for phosphatidic acid phosphatase HAD-type.

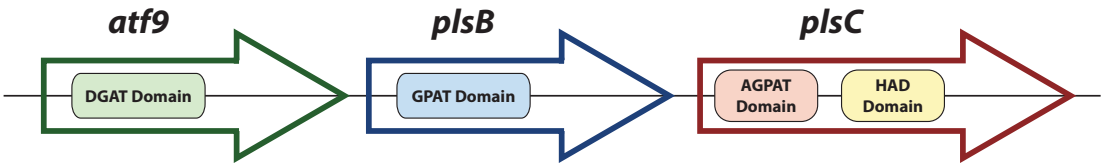

Figure 10. The *atf9-plsB-plsC* operon. Arrows represent the genes and boxes represent the encoded domains. Neither genes nor domains are drawn to scale.

5. Purification and characterization of a putative HAD-type PAP

To test whether the predicted HAD enzymes are involved in TAG biosynthesis in RHA1, we separately cloned the *papH1* and *papH2* genes into the pET15b expression plasmid with an N-terminal polyhistidine affinity tag (His-Tag), and overexpressed them in the *E. coli* strain Rosetta^{TM} 2. Cells were grown at different temperatures and harvested at different times after induction to optimize protein production. Overexpression of *papH1* resulted in the appearance of a 17 kDa protein in the cell lysate (**Fig. 11**), consistent with the predicted molecular weight of the encoded protein. Soluble PapH1 was produced when the cells were incubated at 16-25 °C. However, substantial insoluble protein appeared at temperatures above 25 °C. Overexpression of *papH2* yielded a 29 kDa protein, the predicted size of the gene product. This protein was insoluble under all of the temperature conditions tested (**Fig. 12**).

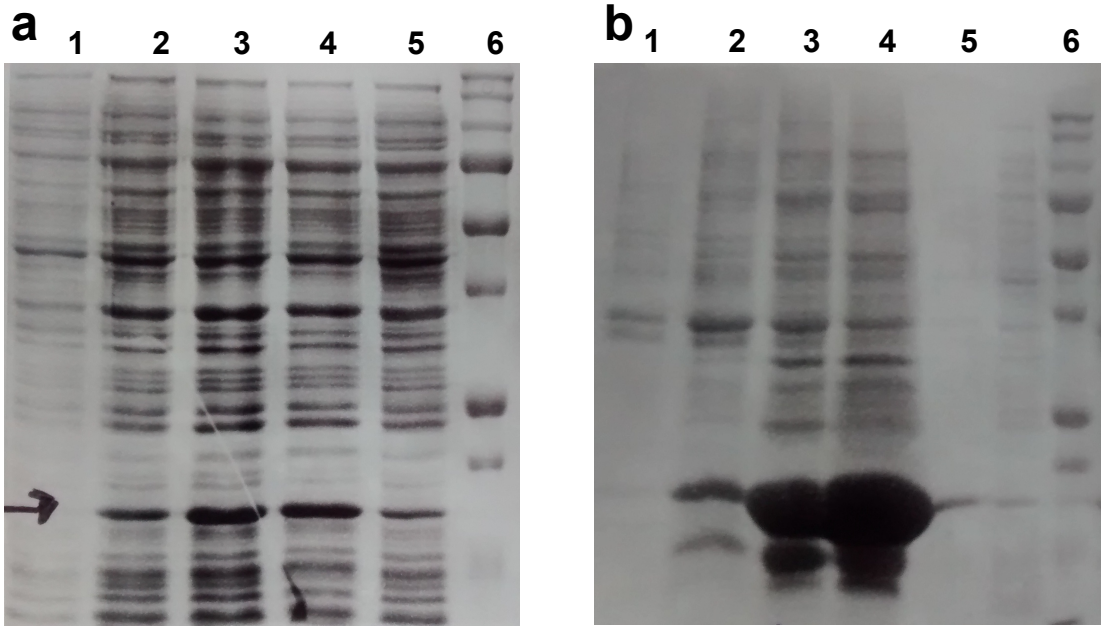

Figure 11. SDS-PAGE analyses of *E. coli* overexpressing *papH1*. a) Soluble fraction of cell lysates. Lane 1, lysate of cells before induction with IPTG. Lanes 2-5, lysate of cells harvested 5 h after induction incubated at 16, 20, 25 and 30 °C, respectively. Lane 6, broad range, prestained molecular weight standard. b) Insoluble fraction of cell lysates. Lane 1-4, lysate of cells harvested 5 h after induction incubated at 16, 20, 25 and 30 °C, respectively. Lane 5, lysate of cells prior to induction with IPTG. Lane 6, broad range prestained molecular weight standard

To purify PapH1, the protein was overproduced at 20 °C. The clarified cell lysate was loaded into a nickel-sepharose column, and washed with buffer containing increasing concentrations of imidazole. The protein started to elute when washed with a 50 mM imidazole buffer. Fractions containing the protein were exchanged into 20mM MOPS buffer and concentrated up to 6.5 mg/ml.

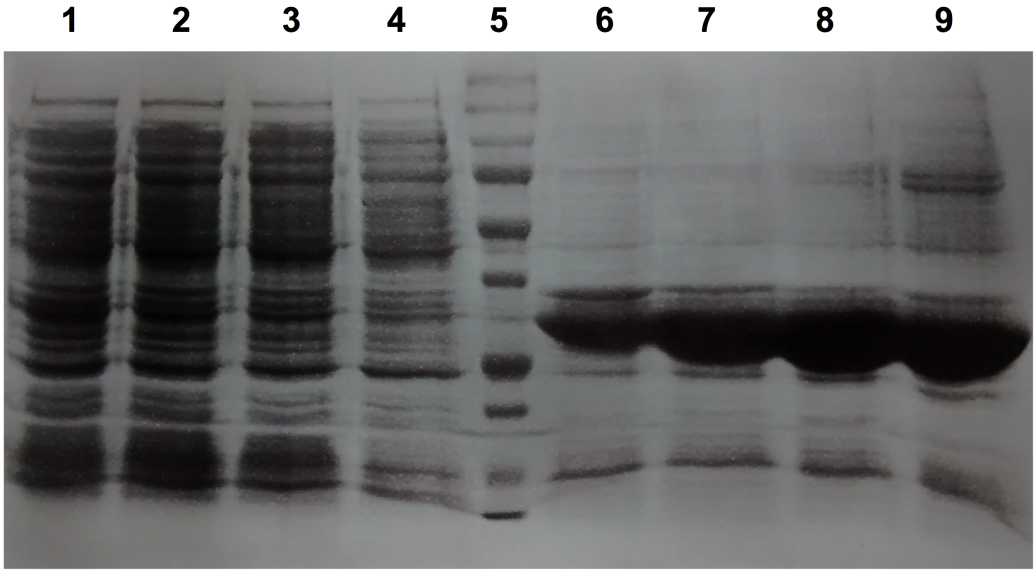

Figure 12. SDS-PAGE analyses of *E. coli* overexpressing *papH2*. Lanes 1-4, soluble fraction of lysate of cells harvested 14h after induction with IPTG, incubated at 20, 25, 30 and 37 °C, respectively. Lane 5 broad range prestained molecular weight standard. Lanes 6-9, insoluble fraction of lysate of cells harvested 14h after induction, incubated at 20, 25, 30 and 37 °C, respectively.

We hypothesized that PapH1 could be involved in TAG biosynthesis by catalyzing the dephosphorylation of phosphatidic acid. To determine phosphatase activity *in vitro*, we adapted a discontinuous assay that follows phosphate release (malachite green) to measure the conversion of dipalmitoyl phosphatidic acid (DPPA) to dipalmitoyl DAG, adding purified PapH1 to catalyze this reaction. Unfortunately, no phosphatase activity was detected (data not shown). Since the predicted active site of PapH1 is close to the N-terminus, the HisTag signal was cleaved using Tobacco Etch Virus protease. Addition of Mg^{2+} to the reaction buffer, which has been described as required for the activity of certain classes of PAPs [35], was also attempted. However, even after these modifications, no DPPA phosphatase activity was detected.

6. Role of non-*atf* Kennedy pathway genes in TAG accumulation in RHA1

We hypothesized that the lack of activity in preparations of purified PapH1 might be due to the requirement of a partner protein, as has been described for some PAPs that need to be in a complex to exhibit phosphatase activity [35]. Therefore, we aimed to test whether these enzymes are involved in TAG biosynthesis *in vivo*. To test the contribution of *papH1*, *papH2*, and *plsC* to TAG accumulation, we ectopically overexpressed them in wild-type RHA1 and investigated their influence under N^- conditions, using a similar approach as in Chapter 3.2 (**Fig. 13**). Overexpression of either *papH2* or *plsC* led to a ~30% decrease in TAG accumulation when cells were harvested 50 hours after ammonium depletion. Overexpression of *papH1* under the same conditions had no detectable effect on TAG accumulation.

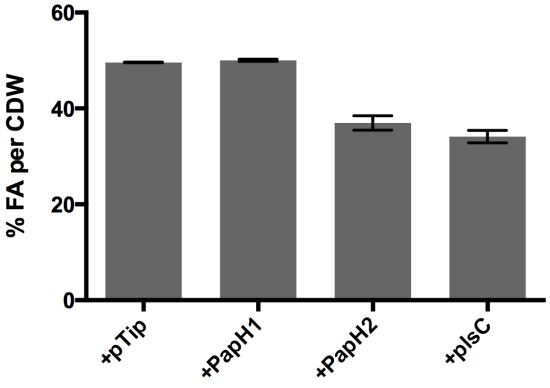

Figure 13. Percentage of FA per CDW of wild-type RHA1 overproducing HAD-type hydrolases. Cells were cultured under N^- conditions and harvested 50 h after ammonia was depleted.

We further investigated the effect of each of *papH1*, *plsC* and *plsB* on TAG biosynthesis by deleting these genes using *sacB*-based homologous recombination as described in Chapter 3.2. As observed for the single *atf* mutants (Chapter 3.2), deletion of either *papH1*, *plsC*, or *plsB*, did not significantly affect TAG accumulation under N^- conditions (**Fig. 14**). On the other hand, deletion of *plsC* and *plsB* under C^- conditions resulted a 45% to 15% decrease, respectively, in TAG content compared to a wild-type strain at stationary phase. Interestingly, the Δ*plsC* mutant accumulated a brown pigment under C^- conditions. This pigment was similar in appearance to oxidized catechol, an intermediate generated in the catabolism of benzoate.

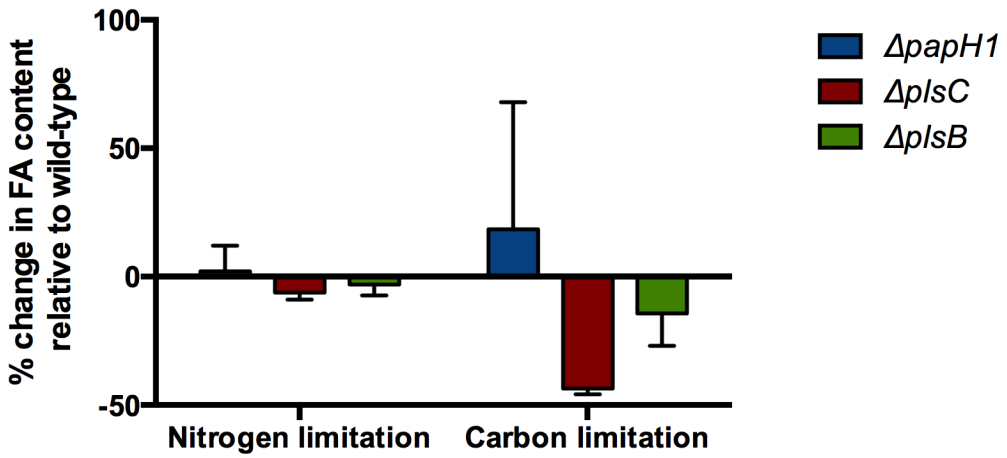

Figure 14. Total FA accumulation in Δ*papH1*, Δ*plsC*, and Δ*plsB* mutants. RHA1 strains were grown on 20 mM benzoate as sole growth substrate under either N^- or C^- conditions. Cells were harvested at 60 h after ammonia was depleted for N^- cultures, and 30 h after benzoate was exhausted for C^- cultures.

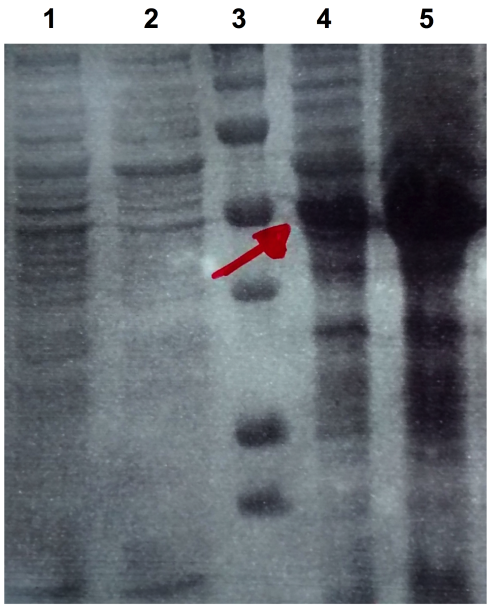

Figure 15. SDS-PAGE of RHA1 producing ht-PlsC. Lanes 1 and 2, soluble fraction of lysates of cells incubated for 8 h at 30 °C after induction with thiostrepton (two replicates). Lane 3, broad range, prestained molecular weight standard. Lanes 4 and 5, insoluble fraction of lysates of cells incubated for 8 h at 30 °C after induction with thiostrepton (two replicates). Red arrow indicates the band corresponding to ht-PlsC.

To further confirm the role of *plsC* in TAG accumulation in RHA1, we ectopically overexpressed it in RHA1 using an N-terminal HisTag. The overproduced protein was highly abundant (**Fig. 15**) but was associated with the insoluble fraction. Attempts to obtain soluble protein by altering the incubation temperature and induction time were unsuccessful. The whole cell lysate was loaded into a Ni-Sepharose column and subjected to a purification protocol described above. SDS-page gel analysis indicated that no soluble protein was obtained. Finally, to investigate the role of *plsB* in TAG biosynthesis, we attempted to measure GPAT activity in whole cell extracts of WT RHA1 and the Δ*plsB* mutant. However, we were unable to detect GPAT activity in any of the strains.

4. DISCUSSION

Oleaginous mycolata contain multiple homologs of the WS/DGATs that catalyze the last step of TAG biosynthesis. Our data establish that these enzymes have somewhat redundant roles in RHA1, but that these roles are not completely overlapping. The clearest case of this in the current study concerns Atf8 and Atf10, which both contribute to TAG biosynthesis under N^- and C^- conditions. More specifically, the *atf10* and *atf8* transcripts were significantly more abundant than any other *atf* transcript during TAG accumulation, most clearly after ammonia depletion under N^- conditions, but also prior to benzoate depletion under C^- conditions. Indeed, *atf10* transcripts were the most abundant of any *atf* under all conditions tested. These RT-qPCR data supersede the RNA-seq data which indicated that *atf8* transcripts were four-fold more abundant than *atf10* transcripts under N^- conditions and that *atf4*, *atf6*, and *atf9* were the most transcribed *atf* genes under C^- conditions [24]. Indeed, measurement of *atf* transcripts abundance on a time-dependent manner provides a more accurate picture of the contribution of different *atf* homologs to TAG accumulation. Most importantly, deletion of both *atf10* and *atf8* was required to significantly diminish TAG accumulation. The contribution of both enzymes is also evident from the FA composition data. By contrast, deletion of *atf6* and *atf9* together had no effect on TAG accumulation under the conditions tested. Despite testing a variety of carbon sources, clones, and harvesting time points, we were unable to replicate our previous finding that the Δ*atf8* mutant accumulates 70% less TAGs than wild-type RHA1 [24]. However, this does not contradict the current conclusion that At8 and Atf10 both contribute to TAG accumulation. The presented data are largely consistent with previous studies in RHA1 and the related strain PD630, that established that *atf8* and *atf10* transcripts and the encoded proteins are highly abundant under lipid storage conditions [24, 31, 32]. In particular, proteomics data suggest that Atf8 and Atf10 are present in similar amounts under these conditions [31].

Nevertheless, Atf8 and Atf10 do not have entirely redundant functions: their overproduction in WT RHA1 yielded opposite phenotypes; they appear to have different substrate specificities; and they may have different subcellular localizations. More particularly, Atf8 augmented TAG accumulation while Atf10 diminished it. The reason

why Atf10 diminishes TAG production, an effect also observed for Atf3, is not clear. It is possible that overexpression of *atf10* induces a metabolic stress that triggers TAG mobilization. This may also be due to the different levels of expression of *atf8* and *atf10* in the pTip vector. Regardless, this effect is consistent with the observation that *atf8* and *atf10* did not complement the Δ*atf8*Δ*atf10* double mutant equally well. Notably, complementation of the double mutant with *atf10* restored the FA profile, suggesting that a functional WS/DGAT was produced. Evidence for the different substrate specificities of Atf8 and Atf10 comes from the FA profile data from the mutants. Thus, the Atf8-overproducing strain had a higher percentage of $C_{15:0}$ and $C_{17:0}$ FAs, suggesting that Atf8 has a higher specificity for odd-numbered acyl-CoAs. $C_{18:1}$ FA was also less abundant in this strain, suggesting that $C_{18:1}$-CoA may be a better substrate for another WS/DGAT, possibly Atf10. Unfortunately, efforts to purify Atf8 have been unsuccessful to date. Finally, Atf8 was found to be associated with lipid droplets in PD630 [32]. Although Atf10 did not appear to be associated with lipid droplets, its subcellular location was not determined. If Atf10 is not associated with lipid droplets, this would suggest two mechanisms by which TAGs are incorporated into these organelles. We cannot either rule out the possibility that structurally different lipid bodies coexist during TAG accumulation in RHA1.

As critical as Atf8 and Atf10 appear to be for TAG accumulation, the data suggest that there are other enzymes involved in TAG accumulation. Thus, although inactivation of *atf8* and *atf10* led to reduced TAG accumulation, the double mutant still contained ~25% CDW in total FAs under N^- conditions. It is likely that other *atf* homologs contribute to TAG biosynthesis under these conditions. Potential candidates include *atf4*, whose transcript became more abundant under prolonged N^- conditions, and *atf7*, whose transcript was up-regulated under N^- conditions [24]. It is also possible that rhodococci contain an *atf*-independent pathway for TAG biosynthesis. Indeed, substantial TAG levels have been reported in mutant or wild-type bacteria containing no *atf* homologs, suggesting the existence of other class of DGATs that may utilize other acyl donors, such as phospholipids [53, 54]. Nevertheless, the available data suggest that redundancy is more prevalent under stress conditions: although deletion of either *atf8* or *atf10* did not

affect TAG accumulation under N^-, TAG content was reduced by 35% and 20%, respectively, under C^- conditions.

Previous reports have variously implicated Atf3 ($Atf1_{PD630}$) Atf6 ($Atf2_{PD630}$) and Atf9 in TAG accumulation based on transcriptional and/or gene deletion data [24, 30-32]. For example, deletion of $atf1_{PD630}$ or $atf2_{PD630}$, corresponding to *atf3* or *atf6* in RHA1, accumulated 30 to 50% less TAG under N^- conditions [29, 30]. However, our study indicates these enzymes don't seem to contribute to TAG accumulation in RHA1 under such conditions: (a) the Δ*atf6*, Δ*atf9* and Δ*atf6*Δ*atf9* mutants had no accumulation defect under any conditions tested and (b) *atf3* transcript levels were very low under N^- conditions. It is unclear why apparently contradictory results were obtained. As noted above, TAG levels in a $\Delta atf1_{PD630}\Delta atf2_{PD630}$ double mutant were comparable to those of the wild-type strain [30], and $Atf1_{PD630}$ appears to have relatively low DGAT activity [29]. Overall, the specific roles of Atf3, Atf6 and Atf9 remain unclear. It is possible that they contribute to the synthesis of structural TAG for the membrane or that they contribute to TAG accumulation under other stresses, such as hypoxia.

The available evidence suggests the existence of functional redundancy in the genes encoding AGPATs in RHA1, since a single *plsC* (*RS27555*) mutant did not have any observable effect in TAG accumulation under N^- conditions. Interestingly, the $plsC_{RHA1}$ homolog in *Mtb*, *Rv2483c*, was predicted to be required for growth in mice based on transposon mutagenesis [55, 56] and a similar mutagenesis study showed that *Rv2483c* contained at least one essential region required for growth *in vitro* [57]. It is possible that this essential region may overlap with either its AGPAT or HAD-type domain. Of the other AGPAT-encoding genes, the *RS05380* transcript was the most abundant under N- conditions in RHA1 [24]. Various mutagenesis studies have established that its *Mtb* homolog, *Rv2182c*, is required for growth *in vitro* [57, 58]. On the other hand, *plsC2* (*RS19670*), which occurs in an operon with another *plsC* homolog and the HAD-encoding *papH2*, was the most upregulated AGPAT in RHA1 [24] under N^- conditions. Interestingly, all three of these AGPATs (*plsC2*, *plsC* and *RS05380*) were associated with lipids droplets in a proteomics study in PD630, although only *plsC2*was more abundant under lipid storage conditions.

The current data extend our understanding about the physiological role of the *atf9-plsB-plsC* operon in mycolata, suggesting that it may fulfill a structural function rather than being directly involved in TAG accumulation: transcripts of each gene were consistently most abundant under C^- conditions [24, 32], and deletion of any one of these genes under lipid storage conditions did not affect TAG accumulation. On the other hand, a Δ*plsC* mutant accumulated a pigment similar in appearance to oxidized catechol. This phenomenon may indicate a perturbation in the composition of the membrane or cell envelope. It is also possible that deletion of *plsC* alters the flux of benzoate through its catabolic pathway. Altogether, this data suggest that the proteins encoded by the *atf9-plsB-plsC* operon are involved in the maintenance of TAGs and other lipid-associated components of the membrane and cell envelope.

The presented data also suggest the existence of an alternative pathway for acylglycerol-phosphate (AGP) biosynthesis in rhodococci, which is common to TAG and phospholipid biosynthesis, since a *plsB* mutant was not significantly deficient in TAG accumulation. Recently, an alternative pathway for AGP production was identified involving two enzymes, PlsX and PlsY. In this system, PlsX transforms an acyl-CoA to an acyl-phosphate and PlsY catalyzes the condensation of the acyl-phosphate and glycerol-phosphate to AGP [59]. However, analysis of representative nocardiaceae (which include the rhodococcus genus) genomes failed to identify either *plsX* or *plsY* homologs in these genomes, suggesting that this system is not present in RHA1. Interestingly, there have been reports of other actinomycetales lacking both *plsB* and *plsXY* homologs, thus raising the possibility that an as-yet-unidentified enzyme sustains the production of AGP to initiate phospholipid and TAG biosynthesis [60]. In this sense, a gene named *plsD* from *Clostridium butyricum*, whose product was closely related with AGPATs and therefore was annotated as *plsC*, was able to complement a *plsB* mutant in *E. coli*, but not a *plsC* mutant [61], suggesting that *plsD* acts as a GPAT instead of an AGPAT. Thus, it is possible that in RHA1, one or more of the eight genes identified as AGPATs based on sequence identify are actually GPATs. Interestingly, a candidate for such an enzyme is *RS19670* or *RS19675,* which occur in an operon and both have amino acid sequence identity with AGPATs.

In this study, we also identified three genes encoding HAD-type hydrolases that could act as PAPs in the biosynthesis of TAGs in mycolata. Many HADs are actually phosphatases [51, 52], and these three genes seem to be involved in TAG biosynthesis in RHA1 based on their operonic arrangement and their gene expression data. Unfortunately, we were unable to obtain biochemical or molecular genetic data to support this hypothesis. It is possible that these HADs require other TAG-related enzymes to perform their function, similar to what occurs during fatty acid or polyketide biosynthesis. Indeed, all of the identified HAD-encoding genes occur in an operon with other TAG biosynthetic genes and one is fused to *plsC*. However, further work is necessary to establish their specific role during TAG biosynthesis.

Finally, our data indicate that TAG accumulation in RHA1 continued for up to five days after ammonia was depleted from the media, and that the WS/DGATs responsible for this accumulation were independent of growth substrate. TAG accumulation has been described in other rhodococci using various growth substrates such as glucose, xylose, L-arabinose, and kraft hardwood pulp hydrolysate, although this accumulation was only monitored for up to three days after ammonium was depleted [19-21, 62]. In these studies, the optimal carbon to nitrogen (C/N) ratio for TAG accumulation was also investigated, but seemed to be highly dependent on the carbon source and nutrient concentration used [19-21]. Our data are also consistent with previous reports that gluconate induces greater TAG accumulation in rhodococci than other non-fatty acid carbon sources [5]. The accumulation of TAGs to 76% CDW in gluconate-grown PD630, the greatest amount of TAGs accumulated from non-fatty acid carbon source reported to date [42], has been attributed to its catabolism through the pentose-phosphate pathway [63], which generates a greater amount of NADPH needed for the *de novo* synthesis of FAs (**Fig. 16**). Finally, our data suggest that the cells decrease in size slightly over this time since they increase in number by an order of magnitude but increase in total biomass (CDW) ~7-fold.

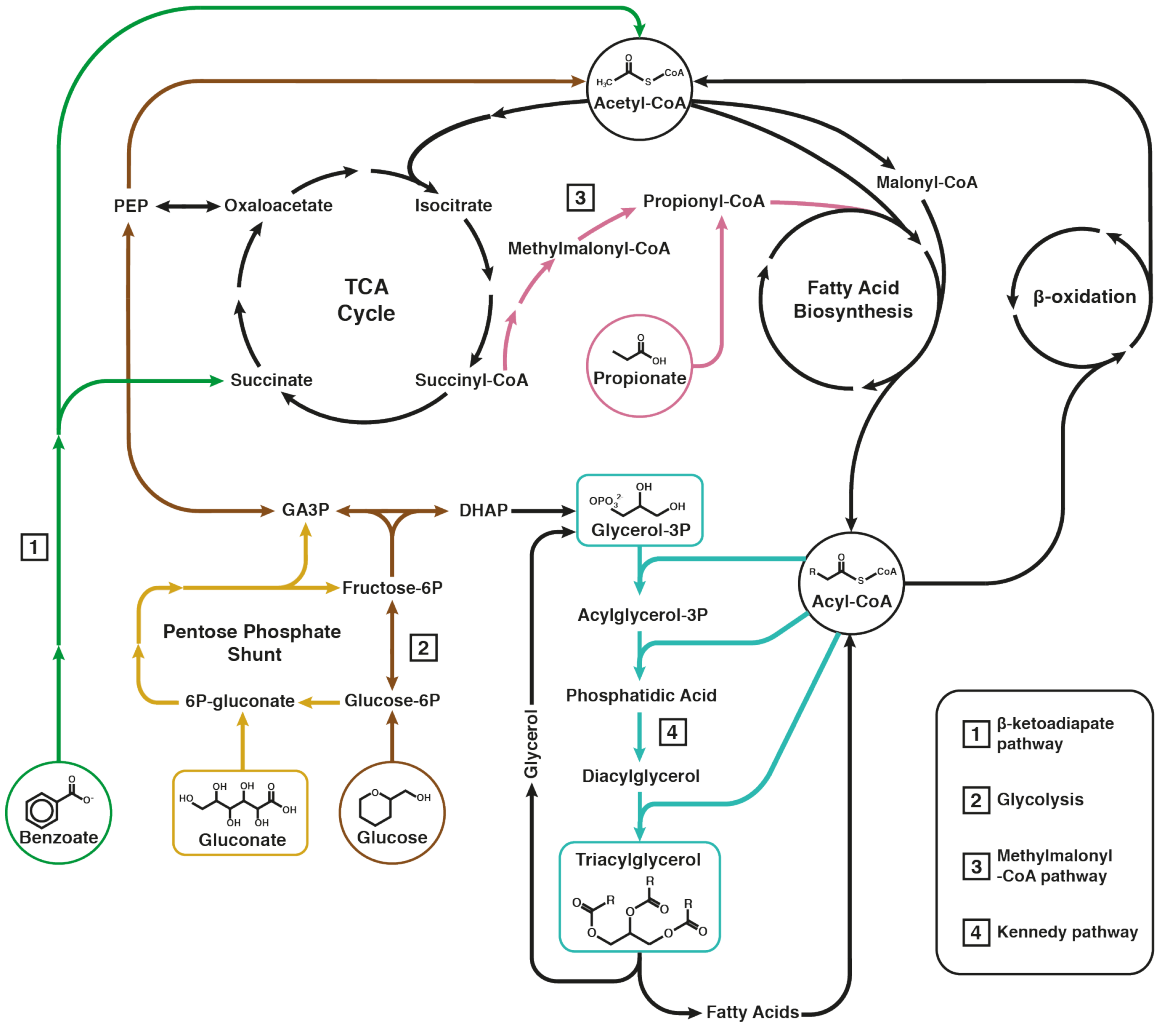

Figure 16. Overview of pathways related to TAG biosynthesis and catabolism of each of the sources used in this study. Relevant routes are coloured as follows: Green, benzoate catabolism. Yellow, gluconate catabolism and pentose phosphate pathway. Brown, Glycolysis. Pink, Propionate catabolism. Blue, TAG biosynthesis pathway. DHAP, Dihydroxyacetone phosphate. GA3P, glyceraldehyde-3-phosphate. PEP, phosphoenolpyruvate.

In this study, we establish that Atf8 and Atf10 are the main WS/DGATs involved in TAG accumulation in *Rhodococcus*, performing somewhat redundant roles. However, there remain many unanswered questions about the final step of TAG biosynthesis in these bacteria. First, it is clear that an as-yet-unidentified process and/or WS/DGAT(s) contribute to TAG biosynthesis. Second, other than Atf8 that appears to be associated with lipid droplets, the subcellular localization of most WS/DGATs, including Atf10, is unknown. Third, the substrate specificity of the different WS/DGATs needs to be determined. Finally, it is possible that WS/DGATs are subject to post-translational regulation, including regulated proteolysis.

Furthermore, we indicate the existence of a certain level of redundancy in the first steps of TAG biosynthesis in *Rhodococcus*, although more work is necessary to establish the physiological role of each enzyme. First, the *plsC* homologs responsible for TAG accumulation under nutrient stress should be identified, perhaps with an approach similar to the one used for the *atf* homologs. Second, the phosphatase activity of the proposed HAD-PAPs needs to be confirmed using a more suitable enzymatic assay. This will help establish the involvement of HAD-PAPs in TAG biosynthesis. Finally, it is clear that PlsB is not the only enzyme in RHA1 that synthesizes AGP. To obtain full understanding of TAG biosynthesis, it is necessary to identify which enzymes are responsible for the synthesis of AGP in RHA1. Addressing these questions is not only important to understand the physiological role of the various TAG-related enzymes in mycolata, but it also essential to engineering these processes for biotechnological applications

REFERENCES

1. Barry III, C.E., et al., *Mycolic acids: structure, biosynthesis and physiological functions.* Progress in Lipid Research, 1998. **37**(2–3): p. 143-179.
2. Sutcliffe, I.C., A.K. Brown, and L.G. Dover, *The Rhodococcal Cell Envelope: Composition, Organisation and Biosynthesis*, in *Biology of Rhodococcus*, M.H. Alvarez, Editor. 2010, Springer Berlin Heidelberg: Berlin, Heidelberg. p. 29-71.
3. Yam, K.C., R. van der Geize, and L.D. Eltis, *Catabolism of Aromatic Compounds and Steroids by Rhodococcus*, in *Biology of Rhodococcus*, M.H. Alvarez, Editor. 2010, Springer Berlin Heidelberg: Berlin, Heidelberg. p. 133-169.
4. Wipperman, M.F., N.S. Sampson, and S.T. Thomas, *Pathogen roid rage: cholesterol utilization by Mycobacterium tuberculosis.* Crit Rev Biochem Mol Biol, 2014. **49**(4): p. 269-93.
5. Hernandez, M.A., et al., *Biosynthesis of storage compounds by Rhodococcus jostii RHA1 and global identification of genes involved in their metabolism.* BMC Genomics, 2008. **9**: p. 600.
6. Alvarez, H.M., *Triacylglycerol and wax ester-accumulating machinery in prokaryotes.* Biochimie, 2016. **120**: p. 28-39.
7. Daniel, J., et al., *Mycobacterium tuberculosis uses host triacylglycerol to accumulate lipid droplets and acquires a dormancy-like phenotype in lipid-loaded macrophages.* PLoS Pathog, 2011. **7**(6): p. e1002093.
8. Ding, Y., et al., *Identification of the major functional proteins of prokaryotic lipid droplets.* J Lipid Res, 2012. **53**(3): p. 399-411.
9. Deb, C., et al., *A novel in vitro multiple-stress dormancy model for Mycobacterium tuberculosis generates a lipid-loaded, drug-tolerant, dormant pathogen.* PLoS One, 2009. **4**(6): p. e6077.
10. Alvarez, H.M. and A. Steinbüchel, *Physiology, Biochemistry, and Molecular Biology of Triacylglycerol Accumulation by Rhodococcus*, in *Biology of Rhodococcus*, M.H. Alvarez, Editor. 2010, Springer Berlin Heidelberg: Berlin, Heidelberg. p. 263-290.
11. Baek, S.-H., A.H. Li, and C.M. Sassetti, *Metabolic Regulation of Mycobacterial Growth and Antibiotic Sensitivity.* PLoS Biol, 2011. **9**(5): p. e1001065.
12. Low, K.L., et al., *Triacylglycerol utilization is required for regrowth of in vitro hypoxic nonreplicating Mycobacterium bovis bacillus Calmette-Guerin.* J Bacteriol, 2009. **191**(16): p. 5037-43.
13. Lestari, S., et al., *Transforming triglycerides and fatty acids into biofuels.* ChemSusChem, 2009. **2**(12): p. 1109-19.
14. Alper, H. and G. Stephanopoulos, *Engineering for biofuels: exploiting innate microbial capacity or importing biosynthetic potential?* Nat Rev Microbiol, 2009. **7**(10): p. 715-23.
15. Holder, J.W., et al., *Comparative and functional genomics of Rhodococcus opacus PD630 for biofuels development.* PLoS Genet, 2011. **7**(9): p. e1002219.
16. Alvarez, H.M., *Biotechnological Production and Significance of Triacylglycerols and Wax Esters*, in *Handbook of Hydrocarbon and Lipid Microbiology*, K.N.

Timmis, Editor. 2010, Springer Berlin Heidelberg: Berlin, Heidelberg. p. 2995-3002.
17. Mycroft, Z., et al., *Biocatalytic conversion of lignin to aromatic dicarboxylic acids in Rhodococcus jostii RHA1 by re-routing aromatic degradation pathways.* Green Chem., 2015. **17**(11): p. 4974-4979.
18. Xiong, X., X. Wang, and S. Chen, *Engineering of a xylose metabolic pathway in Rhodococcus strains.* Appl Environ Microbiol, 2012. **78**(16): p. 5483-91.
19. Kurosawa, K., et al., *High-cell-density batch fermentation of Rhodococcus opacus PD630 using a high glucose concentration for triacylglycerol production.* J Biotechnol, 2010. **147**(3-4): p. 212-8.
20. Kurosawa, K., S.J. Wewetzer, and A.J. Sinskey, *Engineering xylose metabolism in triacylglycerol-producing Rhodococcus opacus for lignocellulosic fuel production.* Biotechnol Biofuels, 2013. **6**(1): p. 134.
21. Kurosawa, K., et al., *Engineering L-arabinose metabolism in triacylglycerol-producing Rhodococcus opacus for lignocellulosic fuel production.* Metab Eng, 2015. **30**: p. 89-95.
22. Wang, B., et al., *Cultivation of lipid-producing bacteria with lignocellulosic biomass: effects of inhibitory compounds of lignocellulosic hydrolysates.* Bioresour Technol, 2014. **161**: p. 162-70.
23. Patrauchan, M.A., et al., *Catabolism of benzoate and phthalate in Rhodococcus sp. strain RHA1: redundancies and convergence.* J Bacteriol, 2005. **187**(12): p. 4050-63.
24. Amara, S., et al., *Characterization of key triacylglycerol biosynthesis processes in rhodococci.* Sci Rep, 2016. **6**: p. 24985.
25. Daniel, J., et al., *Induction of a novel class of diacylglycerol acyltransferases and triacylglycerol accumulation in Mycobacterium tuberculosis as it goes into a dormancy-like state in culture.* J Bacteriol, 2004. **186**(15): p. 5017-30.
26. Röttig, A. and A. Steinbüchel, *Acyltransferases in Bacteria.* Microbiology and Molecular Biology Reviews, 2013. **77**(2): p. 277-321.
27. Kalscheuer, R. and A. Steinbuchel, *A novel bifunctional wax ester synthase/acyl-CoA:diacylglycerol acyltransferase mediates wax ester and triacylglycerol biosynthesis in Acinetobacter calcoaceticus ADP1.* J Biol Chem, 2003. **278**(10): p. 8075-82.
28. Silva, R.A., et al., *Characterization of indigenous Rhodococcus sp. 602, a strain able to accumulate triacylglycerides from naphthyl compounds under nitrogen-starved conditions.* Res Microbiol, 2010. **161**(3): p. 198-207.
29. Alvarez, A.F., et al., *Cloning and characterization of a gene involved in triacylglycerol biosynthesis and identification of additional homologous genes in the oleaginous bacterium Rhodococcus opacus PD630.* Microbiology, 2008. **154**(Pt 8): p. 2327-35.
30. Hernandez, M.A., et al., *The atf2 gene is involved in triacylglycerol biosynthesis and accumulation in the oleaginous Rhodococcus opacus PD630.* Appl Microbiol Biotechnol, 2013. **97**(5): p. 2119-30.
31. Davila Costa, J.S., et al., *Label-free and redox proteomic analyses of the triacylglycerol-accumulating Rhodococcus jostii RHA1.* Microbiology, 2015. **161**(Pt 3): p. 593-610.

32. Chen, Y., et al., *Integrated omics study delineates the dynamics of lipid droplets in Rhodococcus opacus PD630.* Nucleic Acids Res, 2014. **42**(2): p. 1052-64.
33. Zhang, Y.M. and C.O. Rock, *Thematic review series: Glycerolipids. Acyltransferases in bacterial glycerophospholipid synthesis.* J Lipid Res, 2008. **49**(9): p. 1867-74.
34. Hernandez, M.A., et al., *Overexpression of a phosphatidic acid phosphatase type 2 leads to an increase in triacylglycerol production in oleaginous Rhodococcus strains.* Appl Microbiol Biotechnol, 2015. **99**(5): p. 2191-207.
35. Cao, H., et al., *Characterization of a soluble phosphatidic acid phosphatase in bitter melon (Momordica charantia).* PLoS One, 2014. **9**(9): p. e106403.
36. Sambrook, J. and D.W. Russell, *Molecular Cloning: A laboratory Manual*. Vol. 3. 2001, Cold Spring Harbor, NY: Cold Spring Harbor Laboratory Press.
37. Schäfer, A., et al., *Small mobilizable multi-purpose cloning vectors derived from the Escherichia coli plasmids pK18 and pK19: selection of defined deletions in the chromosome of Corynebacterium glutamicum.* Gene, 1994. **145**(1): p. 69-73.
38. Nakashima, N. and T. Tamura, *Isolation and characterization of a rolling-circle-type plasmid from Rhodococcus erythropolis and application of the plasmid to multiple-recombinant-protein expression.* Appl Environ Microbiol, 2004. **70**(9): p. 5557-68.
39. van der Geize, R., et al., *Unmarked gene deletion mutagenesis of kstD, encoding 3-ketosteroid Delta1-dehydrogenase, in Rhodococcus erythropolis SQ1 using sacB as counter-selectable marker.* FEMS Microbiol Lett, 2001. **205**(2): p. 197-202.
40. Koroleff, F., *Determination of Ammonia*, in *Methods of Seawater Analysis*, K. Grasshoff, M. Ehrhardt, and F. Kremling, Editors. 1983, Verlag Chemie: Weinheim. p. 150-157.
41. Biswas, T., et al., *DNA-Dependent ATPase Activity of Bacterial XPB Helicases.* Biochemistry, 2009. **48**(12): p. 2839-2848.
42. Alvarez, H.M., et al., *Formation of intracytoplasmic lipid inclusions by Rhodococcus opacus strain PD630.* Arch Microbiol, 1996. **165**(6): p. 377-86.
43. Hanahan, D., *Studies on transformation of Escherichia coli with plasmids.* Journal of Molecular Biology, 1983. **166**(4): p. 557-580.
44. Simon, R., U. Priefer, and A. Puhler, *A Broad Host Range Mobilization System for In Vivo Genetic Engineering: Transposon Mutagenesis in Gram Negative Bacteria.* Nat Biotech, 1983. **1**(9): p. 784-791.
45. Seto, M., et al., *A Novel Transformation of Polychlorinated Biphenyls by Rhodococcus sp. Strain RHA1.* Appl Environ Microbiol, 1995. **61**(9): p. 3353-8.
46. Smith, D.B. and K.S. Johnson, *Single-step purification of polypeptides expressed in Escherichia coli as fusions with glutathione S-transferase.* Gene, 1988. **67**(1): p. 31-40.
47. Alvarez, H.M., R. Kalscheuer, and A. Steinbüchel, *Accumulation of storage lipids in species of Rhodococcus and Nocardia and effect of inhibitors and polyethylene glycol.* Lipid / Fett, 1997. **99**(7): p. 239-246.
48. Villalba, M.S. and H.M. Alvarez, *Identification of a novel ATP-binding cassette transporter involved in long-chain fatty acid import and its role in triacylglycerol*

accumulation in Rhodococcus jostii RHA1. Microbiology, 2014. **160**(Pt 7): p. 1523-32.
49. Alvarez, H.M., et al., *Biosynthesis of fatty acids and triacylglycerols by 2,6,10,14-tetramethyl pentadecane-grown cells of Nocardia globerula 432.* FEMS Microbiol Lett, 2001. **200**(2): p. 195-200.
50. Indest, K.J., et al., *The effects of putative lipase and wax ester synthase/acyl-CoA:diacylglycerol acyltransferase gene knockouts on triacylglycerol accumulation in Gordonia sp. KTR9.* J Ind Microbiol Biotechnol, 2015. **42**(2): p. 219-27.
51. Kuznetsova, E., et al., *Genome-wide analysis of substrate specificities of the Escherichia coli haloacid dehalogenase-like phosphatase family.* J Biol Chem, 2006. **281**(47): p. 36149-61.
52. Larrouy-Maumus, G., G. Kelly, and L.P. de Carvalho, *Chemical mechanism of glycerol 3-phosphate phosphatase: pH-dependent changes in the rate-limiting step.* Biochemistry, 2014. **53**(1): p. 143-51.
53. Arabolaza, A., et al., *Multiple pathways for triacylglycerol biosynthesis in Streptomyces coelicolor.* Appl Environ Microbiol, 2008. **74**(9): p. 2573-82.
54. Kalscheuer, R., et al., *Analysis of storage lipid accumulation in Alcanivorax borkumensis: Evidence for alternative triacylglycerol biosynthesis routes in bacteria.* J Bacteriol, 2007. **189**(3): p. 918-28.
55. Rengarajan, J., B.R. Bloom, and E.J. Rubin, *Genome-wide requirements for Mycobacterium tuberculosis adaptation and survival in macrophages.* Proc Natl Acad Sci U S A, 2005. **102**(23): p. 8327-32.
56. Sassetti, C.M. and E.J. Rubin, *Genetic requirements for mycobacterial survival during infection.* Proc Natl Acad Sci U S A, 2003. **100**(22): p. 12989-94.
57. Zhang, Y.J., et al., *Global assessment of genomic regions required for growth in Mycobacterium tuberculosis.* PLoS Pathog, 2012. **8**(9): p. e1002946.
58. Griffin, J.E., et al., *High-resolution phenotypic profiling defines genes essential for mycobacterial growth and cholesterol catabolism.* PLoS Pathog, 2011. **7**(9): p. e1002251.
59. Lu, Y.J., et al., *Acyl-phosphates initiate membrane phospholipid synthesis in Gram-positive pathogens.* Mol Cell, 2006. **23**(5): p. 765-72.
60. Lykidis, A., et al., *Genome sequence and analysis of the soil cellulolytic actinomycete Thermobifida fusca YX.* J Bacteriol, 2007. **189**(6): p. 2477-86.
61. Heath, R.J., H. Goldfine, and C.O. Rock, *A gene (plsD) from Clostridium butyricum that functionally substitutes for the sn-glycerol-3-phosphate acyltransferase gene (plsB) of Escherichia coli.* J Bacteriol, 1997. **179**(23): p. 7257-63.
62. Sinskey, A.J., et al., *Production of triacylglycerides, fatty acids, and their derivatives*. 2010, Google Patents.
63. Frunzke, J., et al., *Co-ordinated regulation of gluconate catabolism and glucose uptake in Corynebacterium glutamicum by two functionally equivalent transcriptional regulators, GntR1 and GntR2.* Mol Microbiol, 2008. **67**(2): p. 305-22.